applied sciences

MDPI

Article

Development and Optimization of Self-Healing Cement for CO_2 Injection and Storage Wells: Enhancing Long-Term Wellbore Integrity in Extreme Subsurface Conditions

Ahmed Alsubaih, Kamy Sepehrnoori and Mojdeh Delshad *

Hildebrand Department of Petroleum and Geosystems Engineering, The University of Texas at Austin, Austin, TX 78712, USA; aaa8649@my.utexas.edu (A.A.); kamys@mail.utexas.edu (K.S.)
* Correspondence: delshad@mail.utexas.edu (M.D.)

Abstract: Ensuring long-term wellbore integrity is critical for CO_2 injection and storage operations. Conventional cement degrades in CO_2-rich environments, compromising zonal isolation and increasing leakage risks. This study presents a novel self-healing cement formulation incorporating Barite, Pozzolan, and Chalcedony, optimized using a Design of Experiment (DOE) approach. Geochemical simulations were conducted using PHREEQC and Python to evaluate porosity evolution, mineral stability, and self-sealing efficiency under CO_2 exposure. The results demonstrate that the optimized formulations significantly reduce porosity (within 7–14 days) through the formation of calcium silicate hydrate (C-S-H) gels, enhancing crack sealing and mechanical resilience. Saturation index and phase volume analyses confirm the long-term stability of ECSH2 and Calcite, reinforcing the cement matrix. Compared to conventional cement, the self-healing formulations exhibit improved durability, lower permeability, and superior resistance to CO_2-induced degradation. These findings support the use of self-healing cement in carbon capture and storage (CCS), geothermal energy, and deep-well applications, offering a cost-effective and durable solution for long-term wellbore integrity. However, further experimental validation and field-scale evaluation are needed to confirm the practical performance of these formulations under real-world reservoir conditions.

Keywords: Self Healing; cement; well integrity

check for updates

Academic Editor: Francesco Tornabene

Received: 20 March 2025
Revised: 30 April 2025
Accepted: 6 May 2025
Published: 13 May 2025

Citation: Alsubaih, A.; Sepehrnoori, K.; Delshad, M. Development and Optimization of Self-Healing Cement for CO_2 Injection and Storage Wells: Enhancing Long-Term Wellbore Integrity in Extreme Subsurface Conditions. *Appl. Sci.* **2025**, *15*, 5428. https://doi.org/10.3390/app15105428

Copyright: © 2025 by the authors. Licensee MDPI, Basel, Switzerland. This article is an open access article distributed under the terms and conditions of the Creative Commons Attribution (CC BY) license (https://creativecommons.org/licenses/by/4.0/).

1. Introduction

Cement plays a crucial role in ensuring the integrity of oil and gas wells by providing zonal isolation, structural support, and protection against corrosive fluids. However, exposure to extreme conditions, such as high pressures, thermal cycles, and aggressive wellbore fluids (e.g., CO_2, H_2S, and brines), leads to cement degradation, cracking, and loss of well integrity. The failure of cement sheaths can result in wellbore instability, casing damage, and leakage of hydrocarbons or injected CO_2 in enhanced oil recovery (EOR) and carbon capture and storage (CCS) applications [1–3].

The cement in geothermal wells is exposed to high temperatures between 100 and 400 °C causing deterioration in the structure of the cement. Also, the cement suffers from volumetric shrinkage during pumping in the analysis, and hardening results in microcrack development. Conventional cement is susceptible to a reduction in sealing capacity due to its brittle nature and the weakening bonding with the casing. Leakage in wells typically arises from microcracks that develop and propagate due to factors such as cement job design, downhole stresses, chemical interactions with subsurface fluids, and temperature

fluctuations [4–7]. These defects create undesirable pathways for subsurface fluid migration, often resulting in sustained casing pressure [8].

When CO_2 is dissolved in water, carbonic acid forms and this dissolution leads to a reaction with cement and carbonation that ultimately degrades the cement. The CO_2-brine solution decreases the pH to 4, while the Portland cement has a pH between 13 and 14. Thus, when the cement interacts with the CO_2-brine solution, several precipitation/dissolution reactions will take place. Cement is thermodynamically unstable in CO_2-rich environments and tends to degrade rapidly when exposed to acidic gases. This degradation occurs due to its reaction with calcium hydroxide, which originates from the hydration of calcium silicate phases [9]. Also, they proposed that the Portlandite [$Ca(OH)_2$] and Calcium Silicate Hydrates (CSH) in set cement are gradually depleted, leading to the formation of calcium carbonates (aragonite, vaterite, and/or calcite), amorphous silica gel, and water. It is worth stating that during cement carbonation and degradation, four distinct zones form: the unaltered zone, the portlandite-depleted zone, the calcium carbonate precipitation zone, and the silica gel zone, where calcium leaching and C-S-H decomposition occur. This alteration in the cement can cause a significant leakage issue in both conventional wells and CCS wells.

In recent years, several solutions have been proposed to ensure well integrity, such as implementing proper cement design as a proactive approach or using different cement recipes, such as calcium carbonate precipitant, polymer, and silica gels. Traditionally, as post-job remediation, the oil and gas industry has relied on techniques like top jobs or squeezing cement to address these issues. However, these methods are costly, have a low success rate of approximately 50%, are time-consuming, and require well shutdowns, leading to significant operational expenses [4]. An alternative to performing remedial squeeze jobs is to modify the mechanical properties of the cement so that the downhole sheath will be more durable and resilient to better withstand the stresses that occur from thermal/mechanical cycling. One effective way to modify the mechanical properties of cement is to incorporate elastomer particles. When added to cement slurries, elastomers lower the Young's modulus, making the cement more elastic [10]. This allows the cement sheath to better mitigate the stress and strain state encountered downhole, but the elastomer particles can lower the compressive strength of the cement [11]. There is also a practical limit regarding how much elastomer can be loaded into a particular slurry design. As the elastomer loading increases, the slurry viscosity increases, which increases equivalent circulating density (ECD) and will ultimately require slower pumping rates to reduce the risk of unnecessarily fracturing the formation [12].

Self-healing cement has emerged as an innovative approach to improving the durability of wellbore cement by autonomously repairing cracks and restoring mechanical properties. By incorporating materials that react to environmental triggers—such as water, CO_2, or temperature fluctuations—self-healing cement can mitigate the risks associated with wellbore deterioration. Figure 1 shows the Mechanical properties of various self-healing cement materials, including compressive strength, Young's modulus, and Poisson's ratio obtained from the literature that present significant support to the wells.

Self-healing cement has emerged as a proactive solution capable of autonomously repairing microcracks, mitigating permeability increase, and restoring mechanical strength [11–13]. To build upon these advancements, this study aims to develop and optimize a novel self-healing cement formulation tailored for CO_2 injection and geothermal wells. The primary research objectives are as follows:

1. Design a cement system incorporating Barite, Pozzolan, and Chalcedony/Zeolite that enhances long-term chemical and mechanical stability under CO_2-rich and high-temperature conditions.

2. Employ a Design of Experiment (DOE) framework to systematically determine the most effective compositions for minimizing porosity and enhancing self-sealing performance.
3. Use PHREEQC 3-based geochemical simulations, integrated with Python 3.12 scripting, to evaluate porosity evolution, mineral transformation, and phase volume changes over time.
4. Benchmark the performance of the proposed self-healing formulations against conventional cement to demonstrate improvements in durability and crack resistance.

These objectives aim to establish a validated, simulation-based methodology for designing resilient cement systems that improve wellbore integrity in harsh subsurface environments.

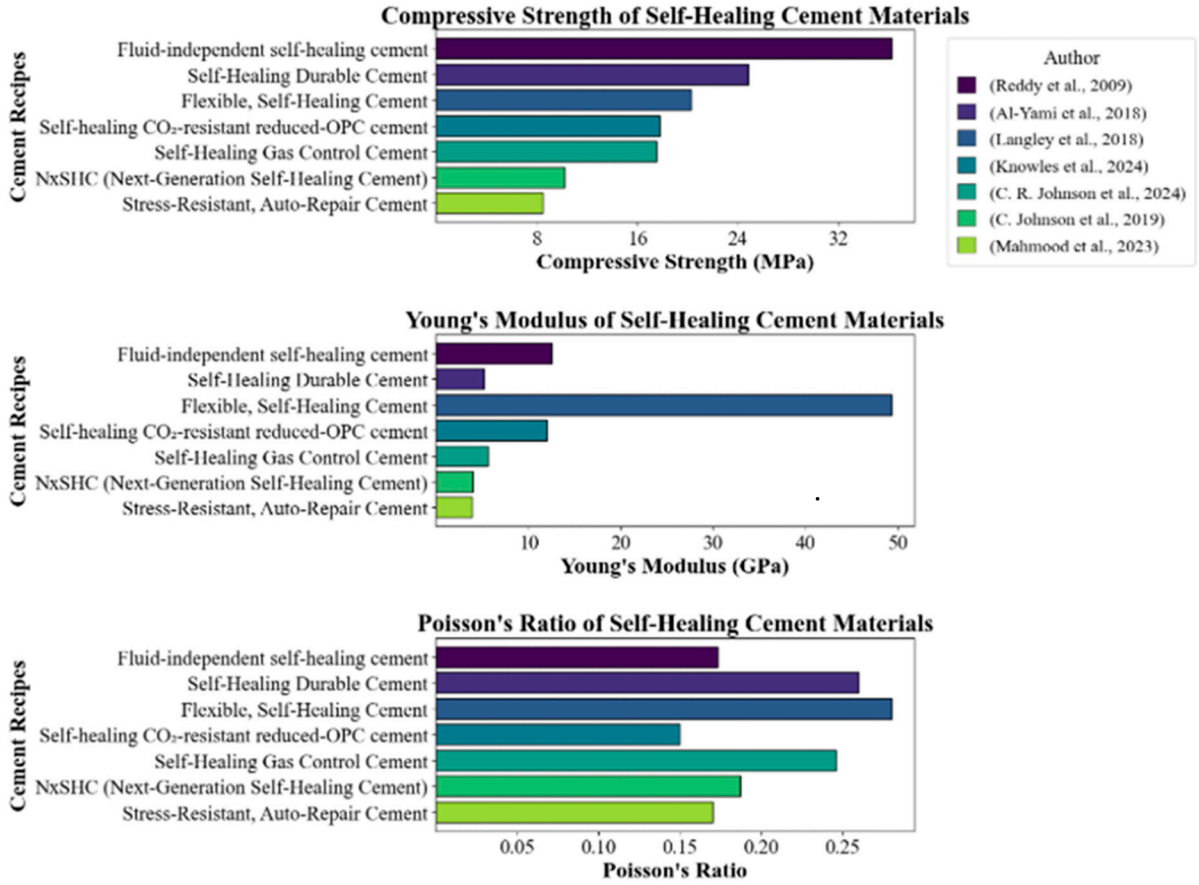


Figure 1. Mechanical properties of various self-healing cement materials, including compressive strength (**top**), Young's modulus (**middle**), and Poisson's ratio (**bottom**). Each bar represents a different cement recipe, color-coded based on the corresponding author [10,14–18].

2. Well Integrity Considerations in High-Temperature and Harsh Environments

Well integrity is influenced by both wellbore and reservoir conditions, including formation fluids, pressure, and temperature variations [19,20]. When the injection fluid is cooler than the formation temperature, or in geothermal wells with significant thermal gradients, casing expansion and contraction occur longitudinally. The casing expansion and shrinkage are prevented and constrained by the cement, creating either compressive or tensile stress in the casing and, consequently, plastic deformation in the cement. These deformations can induce microfractures at the cement-formation and cement-casing interfaces, compromising zonal isolation [21]. Additionally, casing joint decoupling may arise due to extreme drilling conditions, further endangering well integrity.

Corrosion is another critical factor, as it degrades casing strength, leading to failures that threaten long-term well stability. Elevated temperatures exacerbate these issues by reducing the mechanical strength of casing materials, thereby lowering their capacity to withstand burst and collapse pressures. As a result, thermal effects can significantly impair well integrity and, in extreme cases, lead to well failure. Many of these issues originate from cement degradation due to mechanical, thermal, or chemical stresses [22]. At high temperatures, the cement experiences thermal fluctuation in geothermal wells, leading to the development of micro-annuli and micro-cracks due to thermal stresses. Also, cement strength deteriorates either during placement or post-hardening, with the situation worsening in the presence of CO_2 or H_2S, which chemically interact with the cement and accelerate its degradation.

Previous studies have shown that above the critical temperature range of 104–160 °C, cement strength declines as temperature and aging increase [18]. Ref. [23] analyzed casing failure modes, focusing on trapped fluid expansion in the casing-to-casing annulus, suggesting that while tie-back liners could mitigate this issue, they introduce other operational challenges. Proper construction and completion techniques were identified as crucial in minimizing such risks.

Downhole corrosion rates are typically more severe than those in near-surface well sections [24]. Geothermal wells face corrosion issues similar to those encountered in sour oil and gas environments, including pitting, wear, corrosion fatigue, and erosion [25]. To address these concerns, ref. [26] developed Thermal Shock Resistant Cement (TSRC) composites with self-healing properties, which demonstrated an 86% recovery in compressive strength (CS) after a five-day healing period, compared to only 36% recovery in Portland cement under similar conditions.

Recent advancements in self-repairing polymer-cement formulations have been explored, including Calcium Aluminate Phosphate (CaP) cement and Sodium Silicate-Activated Slag (SSAS) cement [27]. These materials offer cost-effective solutions, as they incorporate industrial by-products from coal combustion and steel manufacturing. To enhance cement resistance in acidic environments, ref. [28] recommended incorporating 5% BWOC olivine microparticles, which act as sacrificial materials available for carbonation.

3. Self-Healing Cement

Under reservoir conditions, mechanical and chemical effects can create microcracks, which act as primary pathways for leakage and compromise well integrity, as shown in Figure 2. To enhance the ability of cementitious materials to resist cracking, block the penetration of harmful substances, and prolong their service life, self-healing technology for concrete has been extensively studied. Researchers have introduced various additives, such as fibers and elastomers, into cement slurries to improve the performance of the cement sheath and facilitate the self-healing of cracks. Different self-healing approaches have been developed, including the use of microcapsules, microbes, cementitious materials, nanofillers, geopolymers, and shape-memory alloys [29–32]. Self-healing cement can be categorized into autogenous/natural and autonomous/artificial healing based on the mechanisms involved [5–33]. Autogenous healing occurs due to unreacted cement particles and the carbonation of hydration products, which form calcium carbonate ($CaCO_3$) deposits within cracks in cement-based materials. CO_2-induced self-healing relies on the deposition of calcium carbonate on the surfaces of cement cracks, aiding in their closure. Also, it can occur by blocking cracks by impurities in water or loose cement particles from crack spalling, further hydration of unreacted cement or cementitious materials, and expansion of the hydrated cementitious matrix in crack flanks due to the swelling of calcium silicate hydrate (C–S–H). However, cement recipes with low cement content or water ratio can

improve the cement durability. On the other hand, autonomous healing depends on external healing agents that are not inherently part of the cement-based materials. Authors on autonomous healing have primarily focused on using bacteria, microcapsules, organic or inorganic materials, and superabsorbent polymers, which are employed to seal cracks effectively. Autonomous healing techniques have demonstrated superior performance in repairing cracks compared to most autogenous healing methods, which are typically restricted to addressing cracks with widths narrower than 150 μm [30]. The self-healing capability of cement can be achieved by incorporating bacterial species into the cementitious matrix, as explored by several researchers [6,7,34]. When water penetrates the cracks, it activates dormant microorganisms, which precipitate sufficient microbial calcite. This process effectively seals the cracks and prevents further water intrusion [35,36]. Microencapsulation is a process where tiny particles or liquid droplets are enclosed within an inert shell, protecting the core material from unwanted interactions with the surrounding environment [37,38]. In self-healing applications, microcapsules are embedded into the host matrix during manufacturing. When cracks form, the stress from the crack causes the microcapsule shells to break, releasing the healing agents contained within them. This mechanism allows the material to repair itself effectively. Geopolymer cement is composed of a polymeric Si–O–Al framework, similar to zeolites, but is predominantly amorphous in nature. The term "geopolymer cement" typically refers to cement produced by combining aluminosilicate source materials, such as fly ash or ground granulated blast-furnace slag, with an alkaline solution. This reaction forms silicon-oxo-aluminate chains and networks, giving geopolymer cement its unique properties [39].

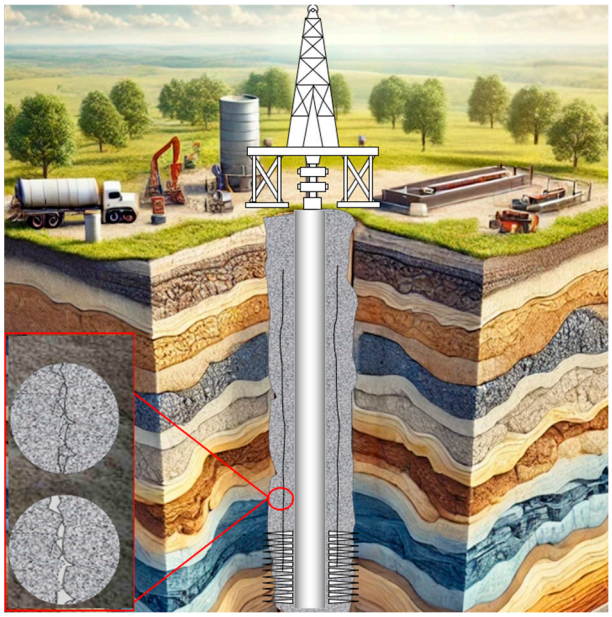


Figure 2. Self-healing cement system in a wellbore. The section shows microcracks before and after self-healing, demonstrating the cement's ability to autonomously repair damage, enhancing durability, zonal isolation, and leakage prevention in subsurface applications.

Pozzolans are widely used in cement formulations to reduce cementation costs and decrease slurry density. Studies have demonstrated that CO_2-saturated brine and supercritical CO_2 can penetrate pozzolanic cement with a 35:65 pozzolan-to-cement volume fraction to a depth of around 170–180 mm over 30 years. This indicates that the inclusion of pozzolans accelerates the rate of CO_2 penetration compared to neat cement [40]. Observations revealed that pozzolanic cement paste reacts significantly faster with CO_2 than neat cement; however, no measurable degradation in the physical properties of pozzolanic

cement was detected [41]. The accelerated penetration in pozzolanic cement is attributed to the increased porosity and higher diffusion rates caused by the pozzolan additives, as well as the reduced portlandite content. This reduction in portlandite minimizes excessive carbonate precipitation, which promotes deeper penetration of CO_2-bearing fluids into the cement matrix [42]. These findings emphasize the critical influence of pozzolan additives in modifying cement microstructure and enhancing its interaction with CO_2, potentially impacting long-term cement integrity in CO_2-rich environments.

The bacterial species loses its healing capacity owing to the higher pH of the concrete. Moreover, the spores of the bacterial species may become damaged because of the shear forces generated, shrinkage during mixing, and drying of the concrete.

Ensuring the long-term integrity of wellbore cement is critical for maintaining zonal isolation, preventing sustained casing pressure (SCP), and mitigating fluid migration in oil and gas wells. Self-healing cement (SHC) technologies have been extensively developed to address these challenges, leveraging various mechanisms such as polymeric additives, elastomers, hydrocarbon-responsive materials, and biomineralization. This review synthesizes advancements in self-healing cement formulations, their underlying mechanisms, and their field applications.

Various self-healing cement technologies enhance wellbore integrity in extreme subsurface conditions. Polymer-based cement, incorporating epoxy resins, improves mechanical strength and reduces permeability by 70% [43], effectively sealing 0.5 mm fractures [44]. Elastomer-enhanced cement increases flexibility and crack resistance, proving effective in HPHT wells (>330 °F, 10,000 psi) [13,45]. Hydrocarbon-responsive cement, such as NxSHC, swells upon contact with hydrocarbons, sealing fractures in high-pressure gas storage wells [15], while water-responsive agents can seal microcracks within 40 min at 2 MPa [46]. CO_2-resistant cement, essential for CCS applications, includes reduced-OPC formulations that maintain integrity under CO_2 exposure [18] and polyethylene glycol-based cement, reducing permeability by 85.5% [47]. Fluid-independent self-healing cement, integrating elastomers, seals microannuli without external fluid activation [14]. Biologically inspired cement (MICP) uses urease-producing bacteria to precipitate $CaCO_3$, improving durability in CO_2-rich and offshore conditions [48]. Advanced technologies, such as microencapsulation and stress-resistant cement, further enhance self-repair, with polyurethane-based microcapsules sealing HPHT wells [49] and stress-resistant cement preventing annular pressure buildup [16]. These innovations significantly improve long-term well integrity across geothermal, CCS, and deep-well applications.

4. Challenges in Self-Healing Cement Technologies

Despite promising advancements, self-healing cement systems face several technical limitations that hinder their widespread deployment. Microencapsulated healing agents, though effective in controlled environments, often rupture during high-shear slurry mixing, rendering them ineffective for post-deployment crack sealing [49]. Additionally, fluid-activated self-healing agents require exposure to wellbore fluids (e.g., water, hydrocarbons) to initiate swelling, complicating slurry design for mixed-fluid environments. Superabsorbent polymers, while beneficial for crack closure, risk premature water absorption, leading to viscosity increases and pumpability issues [14].

Moreover, downhole cyclic thermal and mechanical stresses—such as those experienced during casing expansion/contraction cycles—can induce debonding at casing interfaces and internal fracturing [50]. Biologically inspired approaches, such as microbially induced carbonate precipitation, face further constraints due to bacterial intolerance to high temperatures and weaker healed zones compared to the original cement matrix [51]. Figure 3 shows the healing capability of different materials to the cement, and it can be

observed that most of the self-healing recipes do not cover the size of the crack in the cement in the oil and gas industry, which is reported to be 500 µm [52]. However, only the bacteria can heal the cement in oil and gas cement, and it may not be applicable in reservoir conditions, especially for CO_2 injections.

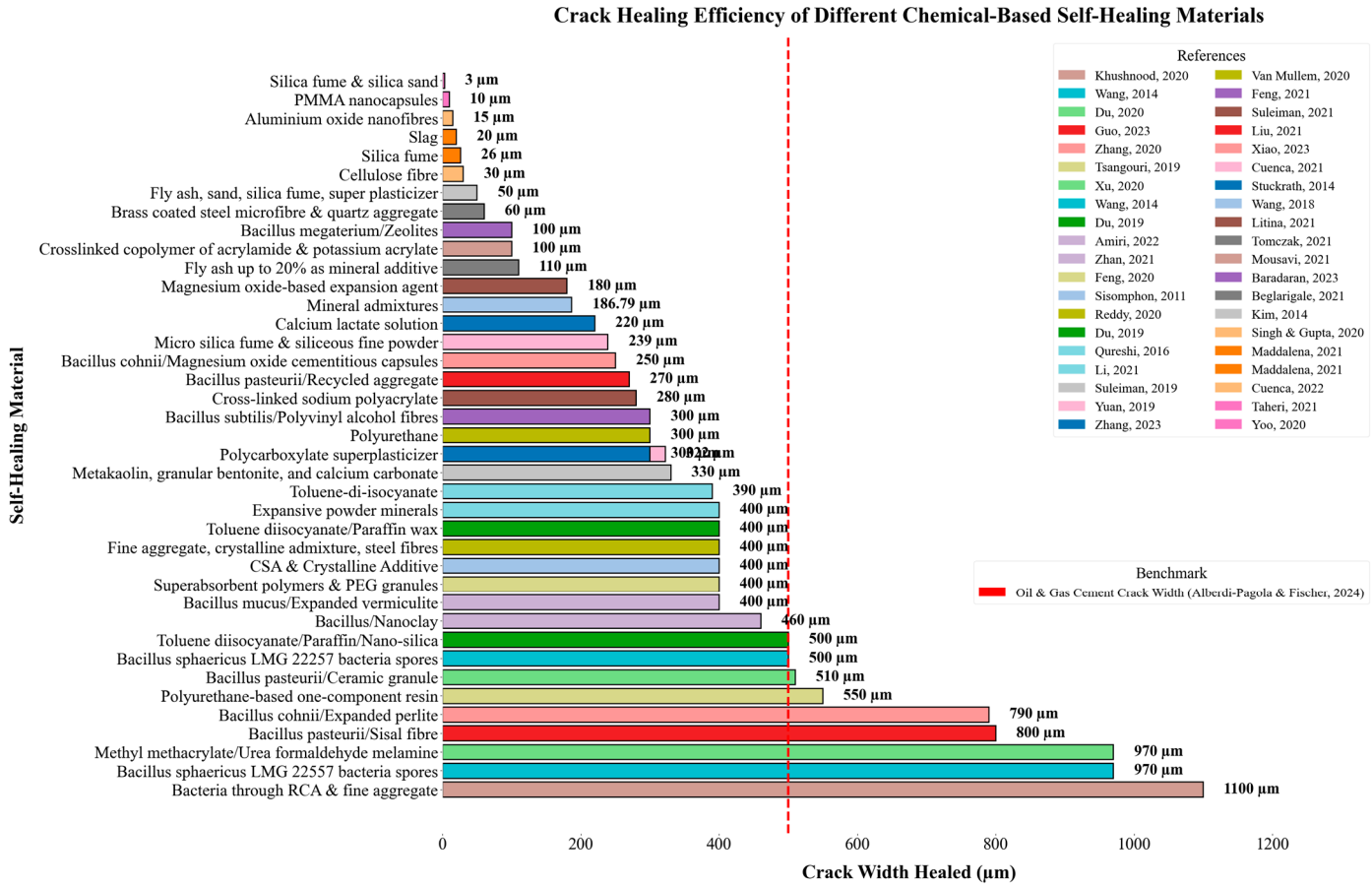


Figure 3. Crack healing efficiency of various chemical-based self-healing materials, showing the maximum crack width that each material can heal. The red dashed line (500 µm) represents the benchmark crack width in oil and gas cement applications, with some materials exceeding this threshold, offering potential for enhanced cement integrity [29,32,33,52–87].

5. Materials and Methods

To address degradation mechanisms in CO_2-rich environments, this study incorporates a mineralogical self-healing concept based on controlled dissolution and re-precipitation. Cement degradation is initiated by the carbonation of portlandite and subsequent decomposition of calcium silicate hydrate (C–S–H) into calcite and silica gel, which weakens the cement matrix [81,88,89]. Initially, calcite precipitation can seal microcracks [90], but prolonged exposure to bicarbonate-rich fluids results in calcium bicarbonate formation and leaching, accelerating porosity increase and structural loss [91]. By leveraging this dissolution–precipitation cycle, the methodology promotes targeted mineral healing to enhance long-term cement integrity.

The methodology for developing a novel self-healing cement follows a structured and systematic approach, integrating experimental design, geochemical modeling, and data analysis to optimize formulations for CO_2-rich subsurface environments. This study evaluates three cement formulations: a novel self-healing cement containing Barite, Pozzolan, and Chalcedony; an advanced self-healing cement incorporating Zeolite for enhanced durability; and conventional cement as a baseline.

The first phase involved designing a self-healing cement system aimed at enhancing mechanical stability, chemical resistance, and self-sealing efficiency. The selected components included Barite (fixed at 3.0 mol, comprising 18.9–24.2 wt.%) to increase density and reduce permeability [92], Pozzolan (0.60–0.75 mol, comprising 43.1–55.4 wt.%) to react with $Ca(OH)_2$ and form secondary C-S-H gels [93], and Chalcedony (0.25–0.40 mol, comprising 23.1–35.9 wt.%) to improve thermal and chemical stability. These components were optimized using a full-factorial Design of Experiment (DOE) approach, selected due to their critical roles in enhancing the geochemical durability of wellbore cement in CO_2-rich environments, consistent with prior studies on cement behavior and mineral reactivity.

The DOE formulation space was structured to maintain slurry density within the operational envelope of 1.88–1.92 g/cm^3, a range commonly employed in field deployments to minimize formation damage and manage hydrostatic pressure. The water-to-cement (w/c) ratio was dynamically adjusted for each formulation to achieve this target density while ensuring realistic mixing conditions. The resulting w/c ratios were consistent with industry standards and closely aligned with the benchmark value of 0.38 recommended in prior literature [89,94]. This methodological choice ensures the designed cement systems are chemically effective and operationally feasible. A detailed summary of the DOE combinations, component mass percentages, cement-to-water proportions, and slurry properties is presented in Appendix A Table A1.

Building upon this foundational formulation, an advanced self-healing cement was developed by incorporating Zeolite (0.10–0.50 mol, corresponding to approximately 12.7–42.7 wt%), known for enhancing CO_2 adsorption and promoting secondary mineral precipitation, thereby further reinforcing the cement matrix. This formulation was similarly optimized through the DOE framework, with simulations automated via a custom Python script interfacing with PHREEQC 3 [95], facilitating batch simulations across varying additive concentrations. PHREEQC 3 is widely used to simulate cement degradation in CO_2-rich environments, enabling accurate prediction of mineral reactions and integrity loss [96–98].

To evaluate self-healing performance, geochemical simulations were executed using PHREEQC 3 and the CEMDATA thermodynamic database, capturing temperature- and pH-dependent solubility behaviors of key cementitious phases (Tables A2 and A3 in Appendix A). Simulations modeled porosity evolution, saturation index (SI) trends, and changes in solid phase volumes over periods ranging from 0.01 days to 30 years, covering both early healing kinetics and long-term mineralogical stabilization. Porosity changes were quantified by tracking dissolution and precipitation of solid phases, normalized against initial solid volumes, thereby reflecting evolving void spaces. This provided a quantitative assessment of self-sealing efficacy throughout the cement system's operational lifetime. The complete simulation workflow is illustrated in Figure 4. The Saturation Index (SI) for each mineral phase was calculated according to Equation (1):

$$SI = Log_{10}\left(\frac{IAP}{K_{SP}}\right) \quad (1)$$

where IAP is the ion activity product and K_{sp} is the solubility product under reservoir temperature and pressure. This formulation was adapted based on PHREEQC modeling practices [95]. SI values were used to assess mineral stability, precipitation, and dissolution behavior throughout the simulation period, enabling evaluation of self-healing potential and long-term chemical durability. The evolution of individual mineral phase volumes was determined by multiplying the simulated number of moles of each phase at each time step, extracted via the KINETICS block output of PHREEQC, by the corresponding molar volume (cm^3/mol) from the CEMDATA thermodynamic database. Phase volumes were

then normalized per 100 g of cementitious material to enable direct comparison across phases. Variations in phase volumes over time provided insight into mineral dissolution–precipitation dynamics, the healing contribution of each phase, and the overall stability of the cement system under CO_2-rich conditions.

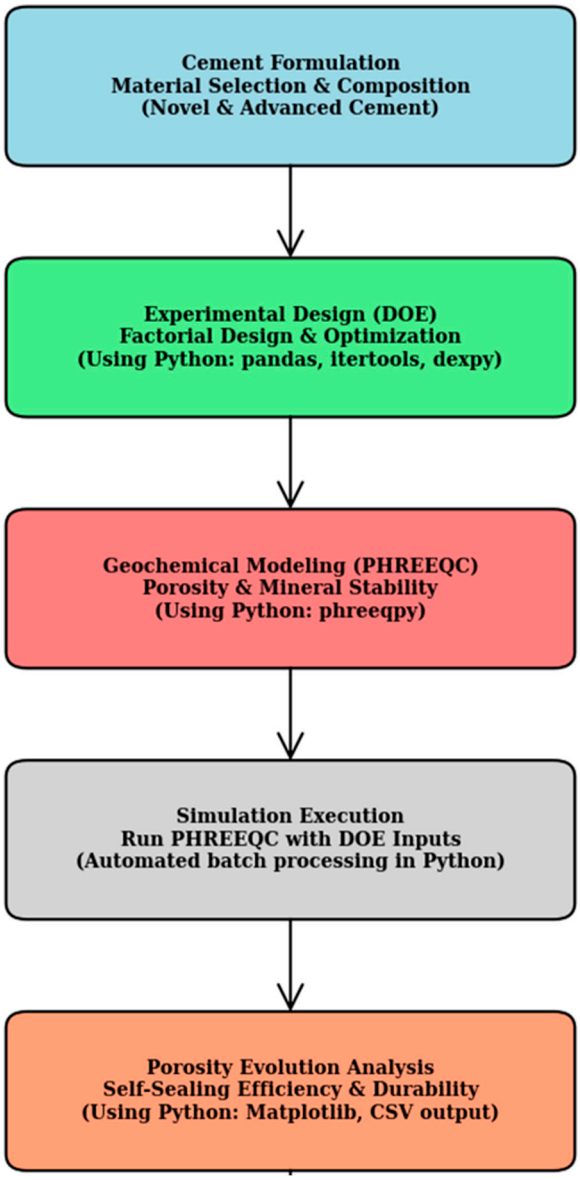


Figure 4. Methodology workflow for self-healing cement development. The workflow illustrates the step-by-step process integrating experimental design, computational geochemical modeling, and data analysis for optimizing self-healing cement formulations. The methodology includes cement formulation, factorial design of experiments (DOE) using Python 3.13 (pandas, itertools, dexpy), geochemical modeling with PHREEQC (phreeqpy library), simulation execution using automated batch processing, and porosity evolution analysis leveraging Matplotlib 3.1 and CSV output processing. This workflow provides a structured approach for evaluating self-sealing efficiency, mineral stability, and long-term durability of cement in CO_2-rich environments.

By integrating experimental design, automated geochemical modeling, and data-driven analysis, this methodology presents a rigorous, scalable framework for developing next-generation self-healing cements tailored for CO_2 sequestration, geothermal applications, and deep-well environments. The resulting cement systems exhibit enhanced

sealing performance, reduced permeability, and improved durability in chemically reactive conditions—supporting safer and more sustainable subsurface energy operations.

6. Results and Discussion

6.1. Porosity Evolution and Self-Healing Efficiency

The porosity evolution of the self-healing cement formulations containing Barite, Pozzolan, and Chalcedony was analyzed over time using PHREEQC geochemical simulations as shown in Figure A1 in the Appendix A. The graph presents porosity changes for multiple DOE (Design of Experiment) combinations, specifically focusing on low-porosity formulations. The logarithmic time scale captures both early-stage reactions and long-term stability trends, providing insights into the self-healing mechanisms of the cement in response to environmental conditions. At the start of the simulation, there is a noticeable drop in porosity, indicating the early-stage reaction of Pozzolan and Chalcedony. This suggests the formation of secondary cementitious compounds, particularly Calcium Silicate Hydrate (C-S-H) gels, which fill initial voids in the cement matrix. The rapid decline in porosity can be attributed to early-stage mineral hydration and precipitation, particularly due to the dissolution of reactive Pozzolan and Chalcedony. Following the initial drop, the porosity stabilizes temporarily, showing only minor fluctuations. This phase indicates a balance between mineral dissolution and precipitation. The slight increase observed around 10^{-2} to 10^{0} days suggests the dissolution of highly soluble phases like Calcite and Portlandite, which may temporarily increase porosity. However, the presence of Pozzolan and Chalcedony ensures the continuous formation of C-S-H phases, preventing excessive porosity growth. A gradual increase in porosity is observed in the long-term phase (10^{2} to 10^{6} days). This can be linked to thermal expansion, mineral conversion, or delayed dissolution of less reactive silica phases. The presence of Chalcedony, which dissolves at a slower rate, may contribute to delayed silica availability, influencing long-term strength. Additionally, the presence of Barite ($BaSO_4$) may be influencing sulfate interactions, leading to slow reprecipitation processes.

Despite slight variations, all low-porosity formulations show consistent behavior, indicating that the cement composition remains structurally stable over extended timeframes. The variations in different DOE combinations suggest that adjustments in Pozzolan and Chalcedony ratios impact reaction kinetics, but overall porosity remains within a narrow range (2.80–2.95%), demonstrating effective self-sealing properties.

6.2. Saturation Index (SI) Evolution of Key Minerals

The saturation index (SI) trends, presented in Figure 5, provide critical insights into mineral stability and precipitation dynamics throughout the simulation period. Key observations include the following:

1. Calcite, Aragonite, and Vaterite exhibit near-equilibrium SI values, indicating a continuous dissolution–precipitation cycle that contributes to crack healing and permeability reduction.
2. Quartz, Chalcedony, and Pozzolan are initially undersaturated, suggesting early-stage silica dissolution, which later stabilizes as these phases reprecipitate into cementitious silicates, reinforcing the matrix.
3. Montmorillonite and Barite remain undersaturated, reflecting limited reactivity under the simulated conditions; however, their presence contributes to cement density stability and resistance against chemical degradation.
4. Portlandite and ECSH2 display a sustained presence, confirming their role in long-term structural reinforcement and enhancing cement integrity.

5. Pyrite and Vivianite remain significantly undersaturated, indicating minimal precipitation in the absence of reducing conditions, which is expected under standard wellbore environments.

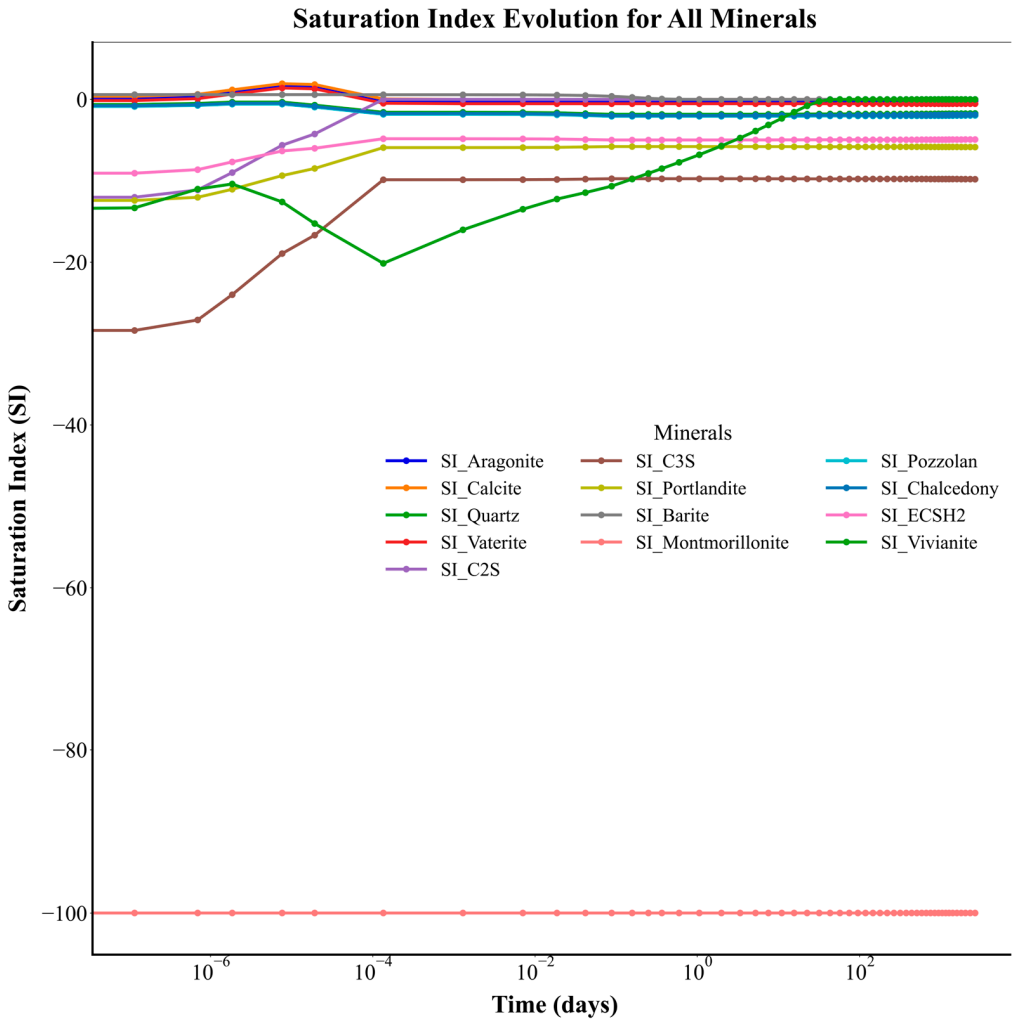


Figure 5. Saturation index evolution of key minerals over time, showing the stability and precipitation-dissolution behavior of self-healing cement components under CO_2-rich conditions, with Aragonite, Calcite, and ECSH2 maintaining near-equilibrium states, ensuring long-term cement integrity.

The overall SI trends confirm that the self-healing cement formulation achieves long-term chemical stability, effectively mitigating excessive dissolution and maintaining structural robustness over extended operational periods. These saturation index trends align closely with the observed porosity evolution and support the mechanistic understanding of the self-healing behavior. Differences of up to two orders of magnitude in the SI values across mineral phases are attributed to variations in mineral solubility, kinetic reactivity, and stability under CO_2-rich conditions. Phases such as Aragonite, Calcite, and ECSH2 tend toward equilibrium, while highly soluble or less reactive phases such as Barite and Montmorillonite remain significantly undersaturated. These trends are consistent with expected mineralogical behavior in reactive wellbore environments. Specifically, the formation of C-S-H, Calcite, and Portlandite—phases with SI values at or above equilibrium—explains both early crack sealing and long-term stability. While Barite remains undersaturated, its role in initial cement density and sulfate buffering remains important. Pozzolan and Chalcedony dissolution supply reactive silica that fuels C-S-H precipitation. The interaction among these mineral phases confirms that the self-healing cement is not only chemically robust but also functionally reliable under sustained CO_2-rich conditions.

6.3. Phase Volume Changes and Mineral Transformations

The phase volume evolution data, illustrated in Figure 6, further supports the robustness of the self-healing cement formulations. Key findings include the following:

1. ECSH2 (a highly reactive C-S-H phase) exhibits consistent volume stability, reaffirming its role in continuous cement reinforcement and crack-sealing functionality.
2. Pozzolan and Chalcedony dissolution contribute to secondary silicate formation, validating their self-healing role through silica gel formation and subsequent precipitation.
3. Calcite and Aragonite display controlled precipitation behavior, suggesting a balance between dissolution and secondary reprecipitation, which is critical for maintaining cement integrity in CO_2-rich environments.
4. Minimal volume loss in key binding phases such as C2S and C3S confirms the structural durability of the cement, as these phases provide essential strength and long-term sealing capabilities in wellbore applications.

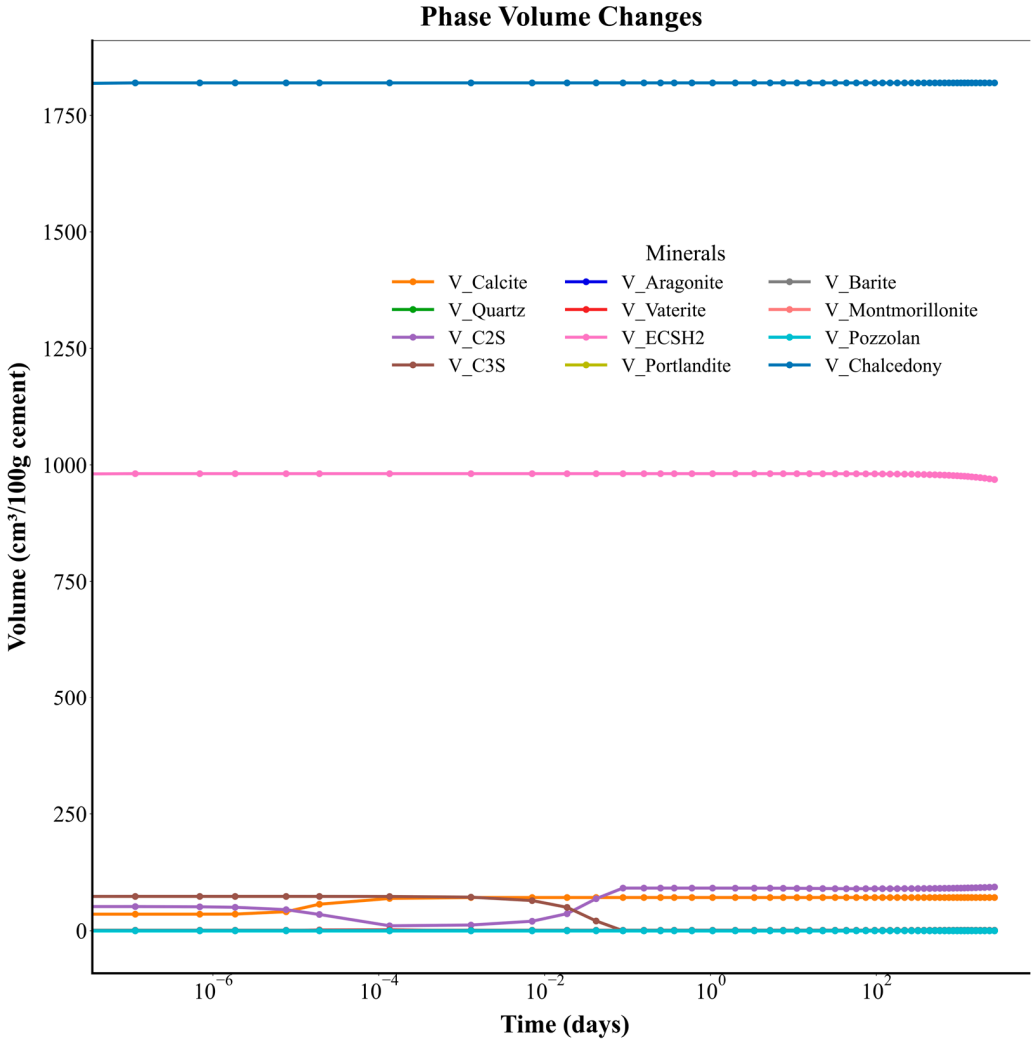


Figure 6. Phase volume changes in key minerals over time, demonstrating the stability of ECSH2 and Chalcedony in self-healing cement formulations under CO_2-rich conditions, ensuring sustained mechanical integrity and resistance to degradation. Observable volume evolution in Calcite, Quartz, C2S, C3S, Vaterite, Portlandite, and Pozzolan confirms active dissolution–precipitation reactions. Barite and Montmorillonite exhibited negligible volume change during the simulation.

Variations in phase volume changes, spanning up to three orders of magnitude, arise from differences in initial phase abundance and mineral dissolution–precipitation kinet-

ics. Phases with higher initial volume fractions, such as C-S-H and Portlandite, show relatively stable behavior, while minor phases exhibit larger relative volume shifts due to their lower starting amounts. These findings validate the effectiveness of the self-healing cement, demonstrating sustained phase stability, mineral transformations conducive to crack healing, and prolonged durability under wellbore conditions.

The results from the porosity evolution analysis emphasize the critical role of advanced self-healing cement formulations in ensuring long-term wellbore integrity in CO_2 injection and storage applications. As depicted in Figure 7, cement formulations containing Barite, Pozzolan, and Zeolite demonstrate superior resistance to CO_2-induced degradation compared to conventional cement, which exhibits a continuous increase in porosity over time when exposed to CO_2-rich reservoir fluids. The Design of Experiment (DOE) approach was employed to optimize the percentage composition of Barite, Pozzolan, and Zeolite, ensuring that the best formulation was identified under severe CO_2 conditions. The DOE findings confirm that specific mineral combinations significantly reduce porosity within the first 7–14 days, enabling early-stage self-sealing while maintaining long-term chemical and mechanical stability.

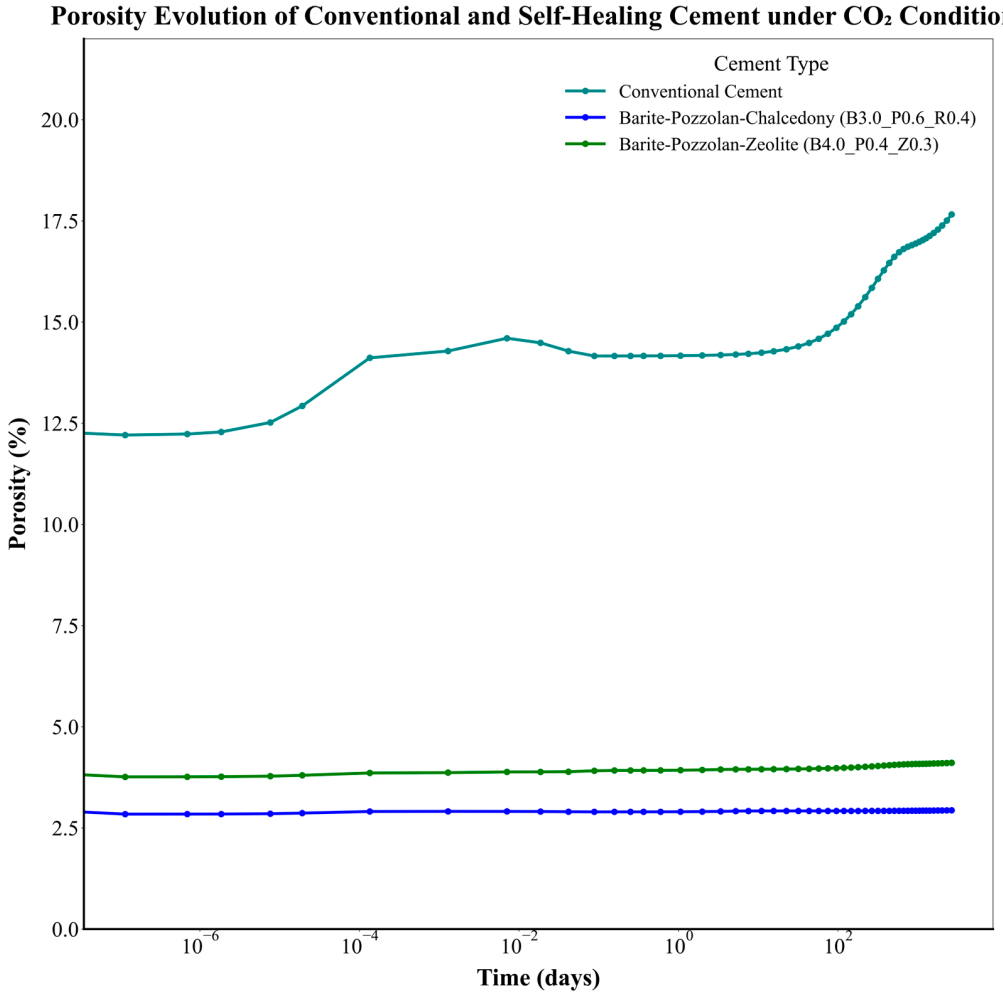


Figure 7. Porosity evolution over time for different cement systems under CO_2 conditions. The conventional cement (teal) shows significant porosity increase (~12–18%), while the Barite–Pozzolan–Chalcedony mix (blue) maintains lower porosity (~3%) and the Barite–Pozzolan–Zeolite mix (green) remains slightly higher (~4%), both with minor increases over time.

The porosity evolution trends of cement formulations (Figure 7) reveal distinct behaviors distinguished by color-coded curves. The self-healing cement systems—Barite-

Pozzolan-Chalcedony (blue) and Barite-Pozzolan-Zeolite (green)—show an initial slight reduction in porosity, followed by gradual stabilization. This behavior is attributed to secondary hydration reactions involving Pozzolan and Zeolite, resulting in the formation of calcium silicate hydrate (C-S-H) gels, which effectively seal microcracks and reduce permeability. Additionally, Barite enhances the density of the cement matrix, limiting CO_2 penetration and improving mechanical stability, thereby reducing the risk of structural failure.

In contrast, the conventional cement (teal curve in Figure 7) fails to maintain porosity stability, exhibiting a continuous increase in porosity exceeding 17% over time. This trend indicates progressive degradation, primarily due to the dissolution of Portlandite and C-S-H phases under CO_2-rich conditions. As these critical cementitious phases deteriorate, the cement structure weakens, accelerating permeability loss and increasing the risk of CO_2 leakage. Unlike the self-healing formulations, conventional cement lacks reactive mineral phases such as Pozzolan and Zeolite that enable self-sealing behavior, making it highly vulnerable to CO_2-induced failure.

The comparative analysis between advanced self-healing cement and conventional cement underscores the importance of mineral optimization in enhancing cement durability in CO_2-rich environments. The integration of Pozzolan and Zeolite not only improves early-stage self-sealing but also ensures long-term resistance against CO_2-induced dissolution and structural weakening.

In comparison with previous research on conventional and alternative self-healing cement systems, the proposed formulation demonstrates several notable advantages. Traditional Portland cement, while widely used, is known to degrade rapidly under CO_2-rich conditions due to the dissolution of Portlandite and C-S-H phases, leading to increased porosity and loss of mechanical strength [9,42]. Prior strategies to enhance cement durability have included polymer-modified cement [43,44], elastomer-based systems [13,45], and microcapsule-reinforced cement [32,49]. However, these approaches often face challenges related to thermal stability, mechanical robustness, or cost-effective scalability. For example, polymer-enhanced systems may exhibit reduced compressive strength or premature healing agent release under high-temperature conditions, limiting their effectiveness in geothermal and CCS wells. In contrast, the cement formulation developed in this study utilizes thermochemically stable mineral additives—Barite, Pozzolan, and Chalcedony—that react in the presence of CO_2, a naturally available trigger in the targeted reservoir environments. This ensures reliable activation without the need for external fluid infiltration or microbial activity. The observed porosity reduction and consistent phase stability demonstrate the superior self-sealing and durability of the proposed formulation under harsh subsurface conditions.

Figure 3 further contextualizes these findings by comparing the healing capability of various self-healing materials across published studies. As illustrated, most materials are limited to healing crack widths significantly smaller than the 500 μm threshold commonly reported in oil and gas applications [52]. Only bacterial-based self-healing systems have demonstrated the ability to seal such large cracks; however, these systems face limitations under actual reservoir conditions. Specifically, microbial self-healing mechanisms may be compromised in CO_2 injection environments due to high pressure, low pH, elevated temperature, and shear forces, which challenge bacterial viability and metabolic activity [48,51,52].

This highlights a critical gap in current self-healing technologies: while several laboratory-scale materials demonstrate promise, few are engineered to withstand the coupled mechanical–chemical stresses encountered in CCS or geothermal wells. The cement formulations proposed in this study offer an inorganic, thermochemically robust

alternative that operates independently of biological or fluid-activated triggers and show early signs of scalability and adaptability under harsh CO_2 reservoir conditions.

Despite these promising results, it is important to recognize the limitations of this work. The findings are based on thermodynamic modeling under controlled CO_2-rich conditions representative of CCS and geothermal reservoirs. However, actual field environments are subject to more complex interactions involving thermal cycles, stress-induced fracture propagation, and fluid heterogeneity. Mechanical deformation, fatigue loading, and long-term durability under cyclic conditions were not captured in this study. Therefore, experimental validation and field-scale assessment are essential to confirm the effectiveness and operational feasibility of the proposed self-healing cement systems.

The porosity evolution over time shows that the Barite–Pozzolan–Zeolite combination (green) maintains a higher porosity (~4%) compared to the Barite–Pozzolan–Chalcedony combination (blue) (~3%) in Figure 7. Both mixtures exhibit slight porosity increases over time, with Zeolite contributing to a more pronounced long-term porosity rise.

7. Conclusions

The development and optimization of self-healing cement formulations incorporating Barite, Pozzolan, and Chalcedony have demonstrated their superior performance in CO_2 injection and storage environments compared to conventional cement. By leveraging a Design of Experiment (DOE) approach, the study systematically identified the optimal compositions that enhance mechanical durability, self-sealing efficiency, and resistance to CO_2-induced degradation.

The porosity evolution analysis revealed that self-healing cement formulations exhibit rapid self-sealing within the first 7–14 days, significantly reducing crack formation and maintaining long-term structural integrity. The inclusion of Pozzolan and Chalcedony facilitated the formation of C-S-H gels, reinforcing the cement matrix and minimizing permeability. Additionally, Barite enhanced density control, thereby limiting fluid migration and improving resistance to mechanical failure in downhole conditions.

Comparative analysis with conventional cement formulations (Figure 7) highlighted their progressive porosity increase, exceeding 17% over time, underscoring their vulnerability to CO_2-rich reservoir fluids. The saturation index (SI) and phase volume changes further validated the stability of self-healing cement, demonstrating that key mineral phases such as ECSH2 and Calcite contribute to long-term strength and crack resistance.

The results of this study provide a strong scientific foundation for the implementation of self-healing cement technology in CO_2 sequestration, geothermal wells, and deep-sea drilling applications. By integrating optimized mineral additives, self-healing cement offers a cost-effective, durable, and environmentally sustainable solution to enhance wellbore integrity, mitigate fluid-induced degradation, and ensure prolonged operational reliability.

These findings reinforce the potential of self-healing cement as a next-generation wellbore sealing material, capable of significantly reducing environmental risks and improving long-term well performance in extreme subsurface conditions. While the geochemical modeling results provide strong theoretical support for self-healing behavior, future work must include laboratory-scale validation under reservoir-relevant conditions. Specifically, experimental studies should evaluate crack sealing performance using split-cylinder or flow-through tests, measure permeability evolution during CO_2 exposure, and quantify mechanical strength recovery after induced microcracking. Additionally, mineralogical analysis via XRD and SEM-EDS should be employed to verify the formation of C-S-H, Calcite, and other healing phases predicted by the model. These experiments will be essential to confirm the predictive accuracy of the PHREEQC simulations and support the practical deployment of the proposed formulations in CCS and geothermal applications.

Looking ahead, the proposed self-healing cement system holds considerable promise for deployment in upcoming carbon capture and storage (CCS) fields, geothermal wells, and permanently abandoned wells that demand long-term zonal isolation. Its activation via CO_2 exposure aligns naturally with conditions found in CCS reservoirs, reducing the need for external triggers or complex activation mechanisms. Nevertheless, several field-scale challenges must be considered, including potential pumpability constraints due to solid additives, modifications to setting times, and variability in healing kinetics across heterogeneous reservoir environments. These challenges may be addressed through tailored slurry design, use of retarders and dispersants, and the integration of real-time monitoring tools such as fiber-optic or acoustic sensing systems to evaluate in situ healing performance. Pilot-scale testing and field demonstrations will be essential next steps to transition this technology from lab-scale validation to operational readiness under actual subsurface conditions.

Author Contributions: Conceptualization, A.A., K.S. and M.D. All authors have read and agreed to the published version of the manuscript.

Funding: This research received no external funding.

Institutional Review Board Statement: Not applicable.

Informed Consent Statement: Not applicable.

Data Availability Statement: The raw data supporting the conclusions of this article will be made available by the authors on request.

Conflicts of Interest: The authors declare no conflict of interest.

Appendix A

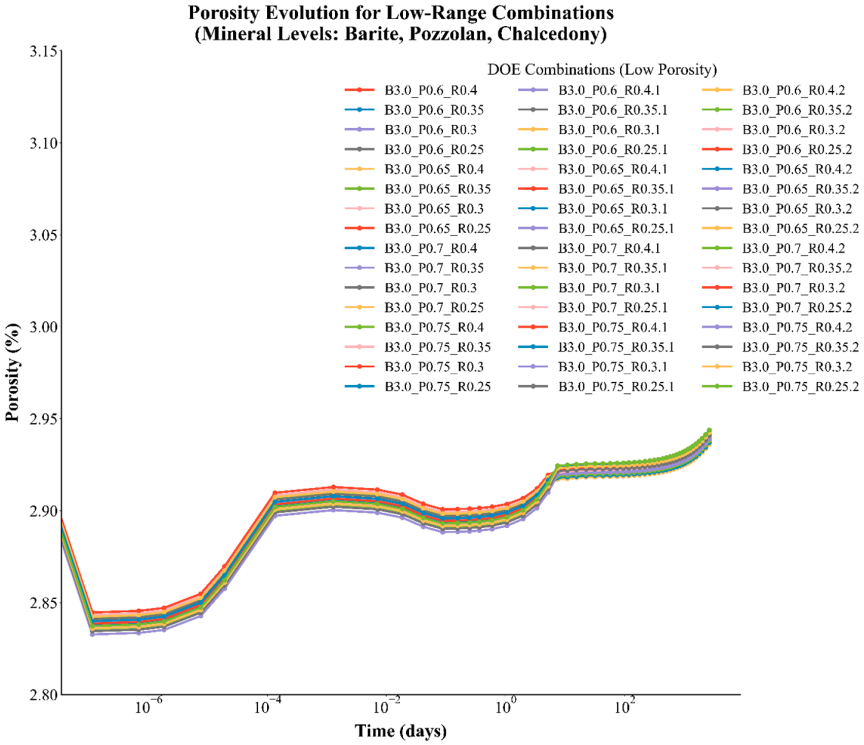


Figure A1. Porosity evolution of self-healing cement formulations incorporating Barite (B), Pozzolan (P), and Chalcedony (R) under CO_2-rich conditions. The graph represents different Design of Experiment (DOE) combinations, demonstrating porosity variations over time.

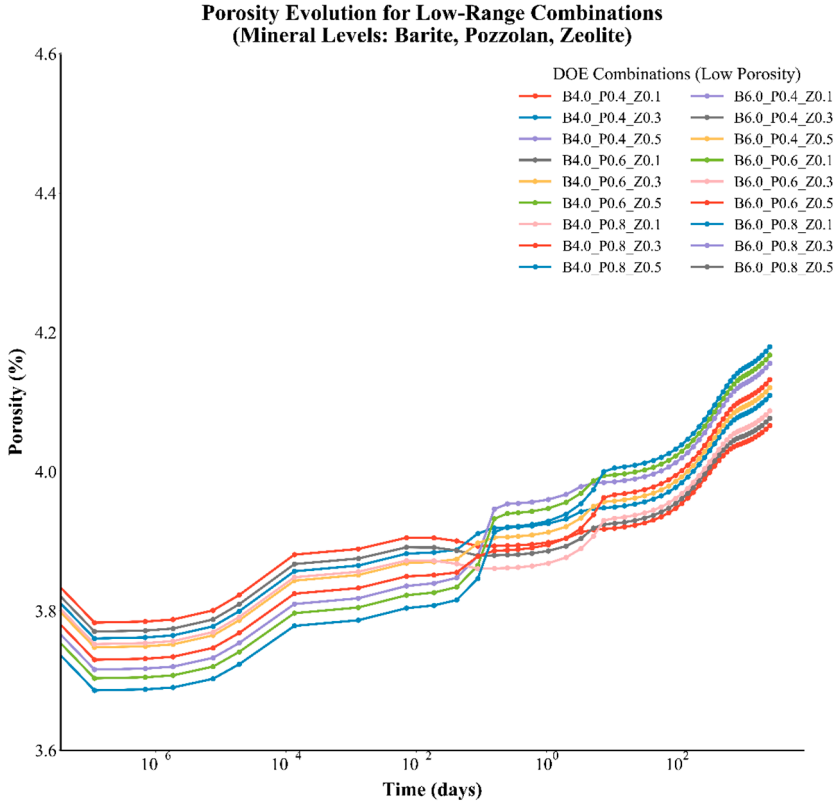


Figure A2. Porosity evolution of self-healing cement formulations containing Barite (B), Pozzolan(P), and Zeolite (Z) under CO_2-rich conditions.

Table A1. Summary of DOE slurry compositions and their physical characteristics. Each row represents a distinct formulation of barite, pozzolan, and chalcedony (in molar quantities), accompanied by the corresponding mass percentage of each mineral. Cement and water masses are calculated based on PHREEQC-defined m_0 values: barite = mol × 0.005, pozzolan = mol × 0.2, and chalcedony = mol × 0.25. Slurry density is fixed at 1.88–1.92 g/cm^3, with water/cement ratio and total slurry volume derived accordingly. These combinations match those presented in the porosity evolution plot (Figure A1).

Barite wt. (%)	Pozzolan wt. (%)	Chalcedony wt. (%)	Cement Mass (g)	Water Mass (g)	Total Volume (cm^3)	Water/Cement Ratio	Slurry Density (g/cm^3)
3.00 (20.9%)	0.60 (43.1%)	0.40 (35.9%)	33.098	11.82	23.64	0.357	1.88
3.00 (21.9%)	0.60 (45.2%)	0.35 (32.9%)	30.472	11.043	21.85	0.362	1.88
3.00 (23.0%)	0.60 (47.4%)	0.30 (29.6%)	27.846	10.265	20.06	0.369	1.88
3.00 (24.2%)	0.60 (49.8%)	0.25 (26.0%)	25.22	9.488	18.27	0.376	1.88
3.00 (20.2%)	0.65 (45.1%)	0.40 (34.7%)	33.736	12.05	24.1	0.357	1.88
3.00 (21.1%)	0.65 (47.1%)	0.35 (31.7%)	31.11	11.272	22.31	0.362	1.88
3.00 (22.1%)	0.65 (49.4%)	0.30 (28.5%)	28.483	10.495	20.51	0.368	1.88
3.00 (23.2%)	0.65 (51.8%)	0.25 (24.9%)	25.857	9.718	18.72	0.376	1.88
3.00 (19.5%)	0.70 (46.9%)	0.40 (33.5%)	34.373	12.279	24.55	0.357	1.88
3.00 (20.4%)	0.70 (49.0%)	0.35 (30.6%)	31.747	11.502	22.76	0.362	1.88
3.00 (21.3%)	0.70 (51.2%)	0.30 (27.4%)	29.121	10.724	20.97	0.368	1.88

Table A1. *Cont.*

Barite wt. (%)	Pozzolan wt. (%)	Chalcedony wt. (%)	Cement Mass (g)	Water Mass (g)	Total Volume (cm^3)	Water/Cement Ratio	Slurry Density (g/cm^3)
3.00 (22.3%)	0.70 (53.7%)	0.25 (24.0%)	26.495	9.947	19.18	0.375	1.88
3.00 (18.9%)	0.75 (48.7%)	0.40 (32.4%)	35.011	12.509	25.01	0.357	1.88
3.00 (19.7%)	0.75 (50.7%)	0.35 (29.6%)	32.385	11.731	23.22	0.362	1.88
3.00 (20.6%)	0.75 (53.0%)	0.30 (26.5%)	29.759	10.954	21.43	0.368	1.88
3.00 (21.5%)	0.75 (55.4%)	0.25 (23.1%)	27.133	10.177	19.64	0.375	1.88
3.00 (19.5%)	0.70 (46.9%)	0.40 (33.5%)	34.373	12.279	24.55	0.357	1.89
3.00 (20.4%)	0.70 (49.0%)	0.35 (30.6%)	31.747	11.502	22.76	0.362	1.89
3.00 (21.3%)	0.70 (51.2%)	0.30 (27.4%)	29.121	10.724	20.97	0.368	1.89
3.00 (22.3%)	0.70 (53.7%)	0.25 (24.0%)	26.495	9.947	19.18	0.375	1.89
3.00 (18.9%)	0.75 (48.7%)	0.40 (32.4%)	35.011	12.509	25.01	0.357	1.89
3.00 (19.7%)	0.75 (50.7%)	0.35 (29.6%)	32.385	11.731	23.22	0.362	1.89
3.00 (20.6%)	0.75 (53.0%)	0.30 (26.5%)	29.759	10.954	21.43	0.368	1.89
3.00 (21.5%)	0.75 (55.4%)	0.25 (23.1%)	27.133	10.177	19.64	0.375	1.89
3.00 (20.9%)	0.60 (43.1%)	0.40 (35.9%)	33.098	11.82	23.64	0.357	1.89
3.00 (21.9%)	0.60 (45.2%)	0.35 (32.9%)	30.472	11.043	21.85	0.362	1.89
3.00 (23.0%)	0.60 (47.4%)	0.30 (29.6%)	27.846	10.265	20.06	0.369	1.89
3.00 (24.2%)	0.60 (49.8%)	0.25 (26.0%)	25.22	9.488	18.27	0.376	1.89
3.00 (20.2%)	0.65 (45.1%)	0.40 (34.7%)	33.736	12.05	24.1	0.357	1.89
3.00 (21.1%)	0.65 (47.1%)	0.35 (31.7%)	31.11	11.272	22.31	0.362	1.89
3.00 (22.1%)	0.65 (49.4%)	0.30 (28.5%)	28.483	10.495	20.51	0.368	1.89
3.00 (23.2%)	0.65 (51.8%)	0.25 (24.9%)	25.857	9.718	18.72	0.376	1.89
3.00 (19.5%)	0.70 (46.9%)	0.40 (33.5%)	34.373	12.279	24.55	0.357	1.9
3.00 (20.4%)	0.70 (49.0%)	0.35 (30.6%)	31.747	11.502	22.76	0.362	1.9
3.00 (21.3%)	0.70 (51.2%)	0.30 (27.4%)	29.121	10.724	20.97	0.368	1.9
3.00 (22.3%)	0.70 (53.7%)	0.25 (24.0%)	26.495	9.947	19.18	0.375	1.9
3.00 (18.9%)	0.75 (48.7%)	0.40 (32.4%)	35.011	12.509	25.01	0.357	1.9
3.00 (19.7%)	0.75 (50.7%)	0.35 (29.6%)	32.385	11.731	23.22	0.362	1.9
3.00 (20.6%)	0.75 (53.0%)	0.30 (26.5%)	29.759	10.954	21.43	0.368	1.9
3.00 (21.5%)	0.75 (55.4%)	0.25 (23.1%)	27.133	10.177	19.64	0.375	1.9
3.00 (20.9%)	0.60 (43.1%)	0.40 (35.9%)	33.098	11.82	23.64	0.357	1.9
3.00 (21.9%)	0.60 (45.2%)	0.35 (32.9%)	30.472	11.043	21.85	0.362	1.9
3.00 (23.0%)	0.60 (47.4%)	0.30 (29.6%)	27.846	10.265	20.06	0.369	1.9
3.00 (24.2%)	0.60 (49.8%)	0.25 (26.0%)	25.22	9.488	18.27	0.376	1.9
3.00 (20.2%)	0.65 (45.1%)	0.40 (34.7%)	33.736	12.05	24.1	0.357	1.9
3.00 (21.1%)	0.65 (47.1%)	0.35 (31.7%)	31.11	11.272	22.31	0.362	1.9
3.00 (22.1%)	0.65 (49.4%)	0.30 (28.5%)	28.483	10.495	20.51	0.368	1.9
3.00 (23.2%)	0.65 (51.8%)	0.25 (24.9%)	25.857	9.718	18.72	0.376	1.9
3.00 (19.5%)	0.70 (46.9%)	0.40 (33.5%)	34.373	12.279	24.55	0.357	1.91
3.00 (20.4%)	0.70 (49.0%)	0.35 (30.6%)	31.747	11.502	22.76	0.362	1.91

Table A1. *Cont.*

Barite wt. (%)	Pozzolan wt. (%)	Chalcedony wt. (%)	Cement Mass (g)	Water Mass (g)	Total Volume (cm^3)	Water/Cement Ratio	Slurry Density (g/cm^3)
3.00 (21.3%)	0.70 (51.2%)	0.30 (27.4%)	29.121	10.724	20.97	0.368	1.91
3.00 (22.3%)	0.70 (53.7%)	0.25 (24.0%)	26.495	9.947	19.18	0.375	1.91
3.00 (18.9%)	0.75 (48.7%)	0.40 (32.4%)	35.011	12.509	25.01	0.357	1.91
3.00 (19.7%)	0.75 (50.7%)	0.35 (29.6%)	32.385	11.731	23.22	0.362	1.91
3.00 (20.6%)	0.75 (53.0%)	0.30 (26.5%)	29.759	10.954	21.43	0.368	1.91
3.00 (21.5%)	0.75 (55.4%)	0.25 (23.1%)	27.133	10.177	19.64	0.375	1.91
3.00 (20.9%)	0.60 (43.1%)	0.40 (35.9%)	33.098	11.82	23.64	0.357	1.91
3.00 (21.9%)	0.60 (45.2%)	0.35 (32.9%)	30.472	11.043	21.85	0.362	1.91
3.00 (23.0%)	0.60 (47.4%)	0.30 (29.6%)	27.846	10.265	20.06	0.369	1.91
3.00 (24.2%)	0.60 (49.8%)	0.25 (26.0%)	25.22	9.488	18.27	0.376	1.91
3.00 (20.2%)	0.65 (45.1%)	0.40 (34.7%)	33.736	12.05	24.1	0.357	1.91
3.00 (21.1%)	0.65 (47.1%)	0.35 (31.7%)	31.11	11.272	22.31	0.362	1.91
3.00 (22.1%)	0.65 (49.4%)	0.30 (28.5%)	28.483	10.495	20.51	0.368	1.91
3.00 (23.2%)	0.65 (51.8%)	0.25 (24.9%)	25.857	9.718	18.72	0.376	1.91
3.00 (19.5%)	0.70 (46.9%)	0.40 (33.5%)	34.373	12.279	24.55	0.357	1.92
3.00 (20.4%)	0.70 (49.0%)	0.35 (30.6%)	31.747	11.502	22.76	0.362	1.92
3.00 (21.3%)	0.70 (51.2%)	0.30 (27.4%)	29.121	10.724	20.97	0.368	1.92
3.00 (22.3%)	0.70 (53.7%)	0.25 (24.0%)	26.495	9.947	19.18	0.375	1.92
3.00 (18.9%)	0.75 (48.7%)	0.40 (32.4%)	35.011	12.509	25.01	0.357	1.92
3.00 (19.7%)	0.75 (50.7%)	0.35 (29.6%)	32.385	11.731	23.22	0.362	1.92
3.00 (20.6%)	0.75 (53.0%)	0.30 (26.5%)	29.759	10.954	21.43	0.368	1.92
3.00 (21.5%)	0.75 (55.4%)	0.25 (23.1%)	27.133	10.177	19.64	0.375	1.92
3.00 (20.9%)	0.60 (43.1%)	0.40 (35.9%)	33.098	11.82	23.64	0.357	1.92
3.00 (21.9%)	0.60 (45.2%)	0.35 (32.9%)	30.472	11.043	21.85	0.362	1.92
3.00 (23.0%)	0.60 (47.4%)	0.30 (29.6%)	27.846	10.265	20.06	0.369	1.92
3.00 (24.2%)	0.60 (49.8%)	0.25 (26.0%)	25.22	9.488	18.27	0.376	1.92
3.00 (20.2%)	0.65 (45.1%)	0.40 (34.7%)	33.736	12.05	24.1	0.357	1.92
3.00 (21.1%)	0.65 (47.1%)	0.35 (31.7%)	31.11	11.272	22.31	0.362	1.92
3.00 (22.1%)	0.65 (49.4%)	0.30 (28.5%)	28.483	10.495	20.51	0.368	1.92
3.00 (23.2%)	0.65 (51.8%)	0.25 (24.9%)	25.857	9.718	18.72	0.376	

Table A2. Aqueous solution composition (SOLUTION 1).

Parameter	Value	Unit	Description
Temperature	110	°C	Reservoir temperature
pH	7	—	Initial fluid pH
Pe	4	—	Redox potential (log scale)
Alkalinity	500	ppm	As HCO_3^-
B	25	ppm	Boron
Ba	2	ppm	Barium

Table A2. *Cont.*

Parameter	Value	Unit	Description
Br	70	ppm	Bromide
Ca	50	ppm	Calcium
Cl	20,000	ppm	Chloride
I	4	ppm	Iodide
K	140	ppm	Potassium
Mg	20	ppm	Magnesium
Na	15,000	ppm	Sodium
P	1.5	ppm	Phosphorus
S (as SO_4^{2-})	300	ppm	Sulfate sulfur (S(VI))
Si	15	ppm	Dissolved silicon
Sr	3	ppm	Strontium
Water mass	100	kg	Total water used in simulation
CO_2(g) partial pressure	280	bar	Imposed CO_2 pressure in gas phase

Table A3. Initial mineral phases (EQUILIBRIUM_PHASES and KINETICS).

Mineral Phase	Initial Amount (mol)	Molar Volume (cm^3/mol)	log K (25 °C)	Rate Constant (Neutral, a2)	Activation Energy (E2, J/mol)
C_2S	0.08	51.79	38.57	1.98×10^{-2}	25,000
C_3S	0.12	73.18	73.41	1.98×10^{-2}	35,000
ECSH1-TobCa	0.08	68	11.02	1.71×10^{-14}	23,000
Calcite	0.05	36.89	−8.48	6.59×10^{-4}	66,000
Quartz	0.1	22.69	−3.98	1.98×10^{-14}	77,000
Montmorillonite	0.05	100	−34.62	1.0×10^{-13}	40,000
Pozzolan	0.60–0.75	22.7	−2.7	0.1×10^{-13}	50,000
Chalcedony	0.25–0.40	22.7	−3.55	13.99×10^{-10}	87,600
Barite	3	50.65	−9.97	1.0×10^{-12}	75,000
Vivianite	0.25	110	−36	1.0×10^{-12}	45,000
Portlandite	1.2	33	22.8	1.0×10^{-8}	25,000
Aragonite	0	34.15	−8.34	1.0×10^{-9}	66,000
Vaterite	0	37.63	−7.91	1.0×10^{-9}	66,000

References

1. Wood, D.A. Well integrity for underground gas storage relating to natural gas, carbon dioxide, and hydrogen. In *Sustainable Natural Gas Drilling: Technologies and Case Studies for the Energy Transition*; Elsevier: Amsterdam, The Netherlands, 2024; pp. 551–576. [CrossRef]
2. Su, X.; Liu, S.; Zhang, L.; Liu, G.; Wang, Y.; Gan, M.; Li, X. Wellbore leakage risk management in CO_2 geological utilization and storage: A review. *Energy Rev.* **2023**, *2*, 100049. [CrossRef]
3. Alsubaih, A.; Sepehrnoori, K.; Delshad, M. Environmental Impacts of Orphaned and Abandoned Wells: Methane Emissions, and Implications for Carbon Storage. *Appl. Sci.* **2024**, *14*, 11518. [CrossRef]
4. Ma, C.; Deng, J.; Wu, R.; Yu, B.; Zhou, Y.; Lin, S. A novel self-healing spacer fluid for sustained casing pressure mitigation. *J. Pet. Sci. Eng.* **2018**, *163*, 722–730. [CrossRef]

5. De Souza, D.J.; Sanchez, L.F.M. Understanding the efficiency of autogenous and autonomous self-healing of conventional concrete mixtures through mechanical and microscopical analysis. *Cem. Concr. Res.* **2023**, *172*, 107219. [CrossRef]
6. De Andrade, J.; Sangesland, S. Cement Sheath Failure Mechanisms: Numerical Estimates to Design for Long-Term Well Integrity. *J. Pet. Sci. Eng.* **2016**, *147*, 682–698. [CrossRef]
7. Kiran, R.; Teodoriu, C.; Dadmohammadi, Y.; Nygaard, R.; Wood, D.; Mokhtari, M.; Salehi, S. Identification and evaluation of well integrity and causes of failure of well integrity barriers (A review). *J. Nat. Gas Sci. Eng.* **2017**, *45*, 511–526. [CrossRef]
8. Yousuf, N.; Olayiwola, O.; Guo, B.; Liu, N. A comprehensive review on the loss of wellbore integrity due to cement failure and available remedial methods. *J. Pet. Sci. Eng.* **2021**, *207*, 109123. [CrossRef]
9. Barlet-Gouédard, V.; Rimmelé, G.; Goffé, B.; Porcherie, O. Well Technologies for CO_2 Geological Storage:CO_2-Resistant Cement. *Oil Gas Sci. Technol.-Revue d'IFPEN* **2007**, *62*, 325–334. [CrossRef]
10. Al-Yami, A.S.; Alqam, M.H.; Riefky, A.; Shafqat, A.U. Self Healing Durable Cement; Development, Lab Testing, and Field Execution. In Proceedings of the SPE/IADC Middle East Drilling Technology Conference and Exhibition, Abu Dhabi, United Arab Emirates, 29–31 January 2018. [CrossRef]
11. Segre, N.; Galves, A.D.; Rodrigues, J.A.; Joekes, I. Tire rubber-cement composites: Effect of slag on properties. *Cerâmica* **2006**, *52*, 283–292. [CrossRef]
12. Wray, B.; Bedford, D.; Leotaud, L.; Hunter, B. The Application of High-Density Elastic Cements to Solve HPHT Challenges in South Texas: The Success Story. In Proceedings of the SPE Annual Technical Conference and Exhibition, New Orleans, LA, USA, 4–7 October 2009; Volume 1, pp. 135–151. [CrossRef]
13. Taoutaou, S.; Bermea, J.A.V.; Bonomi, P.; Elatrache, B.; Pasturel, C.; Brangetto, M. Avoiding Sustained Casing Pressure in Gas wells using Self Healing Cement. In Proceedings of the Society of Petroleum Engineers-International Petroleum Technology Conference 2012, IPTC 2012, Bangkok, Thailand, 7–9 February 2012; Volume 1, pp. 365–373. [CrossRef]
14. Reddy, B.R.; Liang, F.; Fitzgerald, R. Self-Healing Cements that Heal without Dependence on Fluid Contact. In Proceedings of the SPE International Symposium on Oilfield Chemistry, The Woodlands, TX, USA, 20–22 April 2009; Volume 1, pp. 430–436. [CrossRef]
15. Johnson, C.; Gai, A.; Ioan, T.; Landa, J.; Gervasi, G.; Bourgeois, B.; Bouteldja, M. Self-Healing Cement for Long-Term Safe Exploitation of Gas Wells: A New Technology Case Study. In Proceedings of the International Petroleum Technology Conference, Beijing, China, 26–28 March 2019. [CrossRef]
16. Mahmood, A.A.; Jan, U.A.; Khan, A.Y.; Rasheed, H.; Salazar, J.; Shah, K.A.; Khan, S. Step-Change in Cement Design Assures Well Integrity Under Dynamic Stress. In Proceedings of the Society of Petroleum Engineers-SPE 2023 Symposium Compilation, SYM 2023, Richardson, TX, USA, 19 December 2023. [CrossRef]
17. Langley, M.; Cleveland, M.; Eulberg, J.; Hudson, M. Flexible, Self-Healing Cement Eliminates Sustained Casing Pressure in Denver-Julesburg Basin Unconventional Wells. In Proceedings of the Society of Petroleum Engineers-IADC/SPE Drilling Conference and Exhibition, DC 2018, Fort Worth, TX, USA, 6–8 March 2018. [CrossRef]
18. Knowles, J.S.; Johnson, C.R.; Liapunova, N.; Syslak, H. Specialized Carbon Dioxide Self-Healing Cement System Engineered for Carbon Capture and Storage Well in Norwegian Continental Shelf. In Proceedings of the Offshore Technology Conference Asia, OTCA 2024, Kuala Lumpur, Malaysia, 27 February–1 March 2024. [CrossRef]
19. Pyatina, T.; Sugama, T. Aluminum-Rich Cements for High Temperature Geothermal Wells. In Proceedings of the 49th Workshop Geothermal Reservoir Engineering, Stanford, CA, USA, 12-14 February 2024.
20. Wu, Y.; Patel, H.; Salehi, S. Thermal Considerations of Cement Integrity in Geothermal Wells. In Proceedings of the 45th Workshop on Geothermal Reservoir Engineering, Stanford, CA, USA, 10–12 February 2020.
21. Torres, A. Challenges of Casing Design in Geothermal Wells. In Proceedings of the Society of Petroleum Engineers-IADC/SPE Asia Pacific Drilling Technology Conference 2014: Driving Sustainable Growth Through Technology and Innovation, Bangkok, Thailand, 25–27 August 2014; pp. 210–221. [CrossRef]
22. Lambrescu, I.; Abid, K.; Teodoriu, C. Cement-Formation Debonding Due to Temperature Variation in Geothermal Wells: An Intensive Numerical Simulation Assessment. *Energies* **2024**, *17*, 4953. [CrossRef]
23. Southon, J.A. Geothermal Well Design, Construction and Failures. In Proceedings of the World Geothermal Congress, Antalya, Turkey, 24–29 April 2005.
24. Treseder, R.S.; Wieland, R. Down-Hole Corrosion in a Salton Sea Geothermal Well. In *SPE International Conference on Oilfield Chemistry?* Society of Petroleum Engineers: Richardson, TX, USA, 1977; pp. 241–248. [CrossRef]
25. Allahvirdizadeh, P. A review on geothermal wells: Well integrity issues. *J. Clean. Prod.* **2020**, *275*, 124009. [CrossRef]
26. Pyatina, T.; Sugama, T. Cements with supplementary cementitious materials for high-temperature geothermal wells. *Geothermics* **2020**, *86*, 101840. [CrossRef]
27. Sugama, T. *Advanced Cements for Geothermal Wells*; Brookhaven National Laboratory: Upton, NY, USA, 2007. Available online: https://www.osti.gov/biblio/909955 (accessed on 1 April 2025).

28. Olivine-Portland Cement as a Solution to Wellbore Integrity Issues in CO2-Rich Geothermal Reservoirs | GRC 2020 Annual Meeting. Available online: https://grc2020.mygeoenergynow.org/olivine-portland-cement-solution-wellbore-integrity-issues-co2-rich-geothermal-reservoirs (accessed on 30 January 2025).
29. Suleiman, A.R.; Nelson, A.J.; Nehdi, M.L. Visualization and quantification of crack self-healing in cement-based materials incorporating different minerals. *Cem. Concr. Compos.* **2019**, *103*, 49–58. [CrossRef]
30. Arce, G.A.; Hassan, M.M.; Mohammad, L.N.; Rupnow, T. Characterization of Self-Healing Processes Induced by Calcium Nitrate Microcapsules in Cement Mortar. *J. Mater. Civ. Eng.* **2016**, *29*, 04016189. [CrossRef]
31. Gupta, S.; Kua, H.W.; Pang, S.D. Healing cement mortar by immobilization of bacteria in biochar: An integrated approach of self-healing and carbon sequestration. *Cem. Concr. Compos.* **2018**, *86*, 238–254. [CrossRef]
32. Wang, X.F.; Zhang, J.H.; Zhao, W.; Han, R.; Han, N.X.; Xing, F. Permeability and pore structure of microcapsule-based self-healing cementitious composite. *Constr. Build. Mater.* **2018**, *165*, 149–162. [CrossRef]
33. Zhang, W.; Zheng, Q.; Ashour, A.; Han, B. Self-healing cement concrete composites for resilient infrastructures: A review. *Compos B Eng.* **2020**, *189*, 107892. [CrossRef]
34. Azenha, M.; Faria, R.; Ferreira, D. Identification of early-age concrete temperatures and strains: Monitoring and numerical simulation. *Cem. Concr. Compos.* **2009**, *31*, 369–378. [CrossRef]
35. Ruan, S.; Qiu, J.; Weng, Y.; Yang, Y.; Yang, E.H.; Chu, J.; Unluer, C. The use of microbial induced carbonate precipitation in healing cracks within reactive magnesia cement-based blends. *Cem. Concr. Res.* **2019**, *115*, 176–188. [CrossRef]
36. Bhaskar, S.; Hossain, K.M.A.; Lachemi, M.; Wolfaardt, G.; Kroukamp, M.O. Effect of self-healing on strength and durability of zeolite-immobilized bacterial cementitious mortar composites. *Cem. Concr. Compos.* **2017**, *82*, 23–33. [CrossRef]
37. Ghosh, S.K. *Self-Healing Materials: Fundamentals, Design Strategies, and Applications*; Wiley-VCH: Weinheim, Germany, 2009; pp. 1–28. [CrossRef]
38. Youngblood, J.P.; Sottos, N.R. Bioinspired materials for self-cleaning and self-healing. *MRS Bull.* **2008**, *33*, 732–738. [CrossRef]
39. Liu, H.; Chen, W.L.; Pan, R.K.; Shan, Z.T.; Qiao, A.; Drewitt, J.W.E.; Hennet, L.; Jahn, S.; Langstaff, D.P.; Chass, G.A.; et al. From molten calcium aluminates through phase transitions to cement phases. *Adv. Sci.* **2020**, *7*, 1902209. [CrossRef] [PubMed]
40. Kutchko, B.G.; Strazisar, B.R.; Huerta, N.; Lowry, G.V.; Dzombak, D.A.; Thaulow, N. CO_2 reaction with hydrated class H well cement under geologic sequestration conditions: Effects of flyash admixtures. *Environ. Sci. Technol.* **2009**, *43*, 3947–3952. [CrossRef] [PubMed]
41. Strazisar, B.; Kutchko, B.; Huerta, N. Chemical Reactions of Wellbore Cement Under CO_2 Storage Conditions: Effects of Cement Additives. *Energy Procedia* **2009**, *1*, 3603–3607. [CrossRef]
42. Carey, J.W. Geochemistry of Wellbore Integrity in CO_2 Sequestration: Portland Cement-Steel-Brine-CO_2 Interactions. *Rev. Miner. Geochem.* **2013**, *77*, 505–539. [CrossRef]
43. Rod, K.A.; Fernandez, C.A.; Nguyen, M.T.; Gardiner, J.B.; Huerta, N.J.; Glezakou, V.A.; Varga, T.; Rousseau, R.; Koech, P.K. Polymer-cement composites with adhesion and re-adhesion (healing) to casing capability for geothermal wellbore applications. *Cem. Concr. Compos.* **2020**, *107*, 103490. [CrossRef]
44. Childers, M.I.; Nguyen, M.T.; Rod, K.A.; Koech, P.K.; Um, W.; Chun, J.; Glezakou, V.A.; Linn, D.; Roosendaal, T.J.; Wietsma, T.W.; et al. Polymer-Cement Composites with Self-Healing Ability for Geothermal and Fossil Energy Applications. *Chem. Mater.* **2017**, *29*, 4708–4718. [CrossRef]
45. Muhammad, A.; Taoutaou, S.; Shafqat, A.U.; Noor, S.M.; Salehpour, A. The Use of Self-Healing Cement to Ensure Long-Term Zonal Isolation for HPHT Wells Subject to Hydraulic Fracturing Operations in Pakistan. In Proceedings of the International Petroleum Technology Conference (IPTC), Doha, Qatar, 7–9 December 2009; International Petroleum Technology Conference: Richardson, TX, USA, 2009. [CrossRef]
46. Xin, H.; Yang, K.; Zhang, M.; Deng, Q.; Zeng, J.; Zou, J.; Sun, F. Exploratory Research on Water-Channeling Self-Healing Agent for Cementing. In Proceedings of the ISOPE International Ocean and Polar Engineering Conference, Shanghai, China, 11–16 October 2020.
47. Peng, Z.G.; Yu, C.Y.; Feng, Q.; Zheng, Y.; Huo, J.H.; Wu, J.R. Synthesis, characterisation and application of self-healing material in oil well cement for healing microcracks. *Adv. Cem. Res.* **2019**, *32*, 519–526. [CrossRef]
48. Noshi, C.I.; Schubert, J.J. A Novel Microbially Induced Self-Healing Cement/Concrete for Underwater Concrete Offshore Structures. In Proceedings of the SPE/IADC Drilling Conference and Exhibition, Hague, The Netherlands, 5–7 March 2019. [CrossRef]
49. Baltaeva, M.; Stamer, K.; Orlov, M. Complex Micro-Containers (CMC) Transporting Compartmentalized Reaction Mixture for Self-Healing Cement. In Proceedings of the SPE Middle East Oil and Gas Show and Conference, Manama, Bahrain, 19–21 February 2023. [CrossRef]
50. Ravi, K.; Bosma, M.; Hunter, L. Optimizing the Cement Sheath Design in HPHT Shearwater Field. In Proceedings of the SPE/IADC Drilling Conference and Exhibition, Amsterdam, The Netherlands, 19–21 February 2003. [CrossRef]

51. Noshi, C.I.; Schubert, J.J. Self-Healing Biocement and Its Potential Applications in Cementing and Sand-Consolidation Jobs: A Review Targeted at the Oil and Gas Industry. In Proceedings of the Society of Petroleum Engineers-SPE Liquids-Rich Basins Conference-North America 2018, LRBC 2018, Midland, TX, USA, 5–6 September 2018. [CrossRef]
52. Alberdi-Pagola, P.; Fischer, G. Quantification of Casing Expansion-Induced Cracking in Oilwell Cement Sheaths. *SPE J.* **2024**, *29*, 714–724. [CrossRef]
53. Wang, J.Y.; Soens, H.; Verstraete, W.; De Belie, N. Self-healing concrete by use of microencapsulated bacterial spores. *Cem. Concr. Res.* **2014**, *56*, 139–152. [CrossRef]
54. Stuckrath, C.; Serpell, R.; Valenzuela, L.M.; Lopez, M. Quantification of chemical and biological calcium carbonate precipitation: Performance of self-healing in reinforced mortar containing chemical admixtures. *Cem. Concr. Compos.* **2014**, *50*, 10–15. [CrossRef]
55. Zhang, T.; Zhao, B.; Shi, L.; Yang, K.; Li, P.; Sun, F.; Zeng, J.; Hou, W.; Yang, L. Research and Application of Ultra-High Density Natural Gas Self-Healing Slurry System. In Proceedings of the ISOPE International Ocean and Polar Engineering Conference, Ottawa, ON, Canada, 18–23 June 2023.
56. Maddalena, R.; Taha, H.; Gardner, D. Self-healing potential of supplementary cementitious materials in cement mortars: Sorptivity and pore structure. *Dev. Built Environ.* **2021**, *6*, 100044. [CrossRef]
57. Cuenca, E.; Criado, M.; Giménez, M.; Alonso, M.C.; Ferrara, L. Effects of Alumina Nanofibers and Cellulose Nanocrystals on Durability and Self-Healing Capacity of Ultrahigh-Performance Fiber-Reinforced Concretes. *J. Mater. Civ. Eng.* **2022**, *34*, 04022154. [CrossRef]
58. Du, W.; Yu, J.; Gu, Y.; Li, Y.; Han, X.; Liu, Q. Preparation and application of microcapsules containing toluene-di-isocyanate for self-healing of concrete. *Constr. Build. Mater.* **2019**, *202*, 762–769. [CrossRef]
59. Xu, J.; Tang, Y.; Wang, X.; Wang, Z.; Yao, W. Application of ureolysis-based microbial $CaCO_3$ precipitation in self-healing of concrete and inhibition of reinforcement corrosion. *Constr. Build. Mater.* **2020**, *265*, 120364. [CrossRef]
60. Liu, C.; Xing, L.; Liu, H.; Huang, W.; Nong, X.; Xu, X. Experimental on repair performance and complete stress-strain curve of self-healing recycled concrete under uniaxial loading. *Constr. Build. Mater.* **2021**, *285*, 122900. [CrossRef]
61. Guo, Y.; Xiang, K.; Wang, H.; Liu, X.; Ye, Q.; Wang, X. Experimental study on self-healing and mechanical properties of sisal fiber-loaded microbial concrete. *Mater. Res. Express* **2023**, *10*, 045701. [CrossRef]
62. Feng, J.; Chen, B.; Sun, W.; Wang, Y. Microbial induced calcium carbonate precipitation study using Bacillus subtilis with application to self-healing concrete preparation and characterization. *Constr. Build. Mater.* **2021**, *280*, 122460. [CrossRef]
63. Baradaran, M.; Sadeghpour, M. Effect of bacteria on the self-healing ability of concrete containing zeolite. *Innov. Infrastruct. Solut.* **2023**, *8*, 256. [CrossRef]
64. Amiri, Y.; Hassaninasab, S.; Chehri, K.; Zahedi, M. Investigating the effect of adding bacillus bacteria and nano-clay on cement mortar properties. *Case Stud. Constr. Mater.* **2022**, *17*, e01167. [CrossRef]
65. Zhan, Q.; Zhou, J.; Wang, S.; Su, Y.; Liu, B.; Yu, X.; Pan, Z.; Qian, C. Crack self-healing of cement-based materials by microorganisms immobilized in expanded vermiculite. *Constr. Build. Mater.* **2021**, *272*, 121610. [CrossRef]
66. Litina, C.; Bumanis, G.; Anglani, G.; Dudek, M.; Maddalena, R.; Amenta, M.; Papaioannou, S.; Pérez, G.; García Calvo, J.L.; Asensio, E.; et al. Evaluation of Methodologies for Assessing Self-Healing Performance of Concrete with Mineral Expansive Agents: An Interlaboratory Study. *Materials* **2021**, *14*, 2024. [CrossRef] [PubMed]
67. Khushnood, R.A.; Qureshi, Z.A.; Shaheen, N.; Ali, S. Bio-mineralized self-healing recycled aggregate concrete for sustainable infrastructure. *Sci. Total Environ.* **2020**, *703*, 135007. [CrossRef] [PubMed]
68. Taheri, S.; Clark, S.M. Preparation of Self-healing Additives for Concrete via Miniemulsion Polymerization: Formulation and Production Challenges. *Int. J. Concr. Struct. Mater.* **2021**, *15*, 8. [CrossRef]
69. Yoo, D.Y.; Shin, W.; Chun, B.; Banthia, N. Assessment of steel fiber corrosion in self-healed ultra-high-performance fiber-reinforced concrete and its effect on tensile performance. *Cem. Concr. Res.* **2020**, *133*, 106091. [CrossRef]
70. Cuenca, E.; Serna, P. Autogenous Self-Healing Capacity of Early-Age Ultra-High-Performance Fiber-Reinforced Concrete. *Sustainability* **2021**, *13*, 3061. [CrossRef]
71. Yuan, L.; Chen, S.; Wang, S.; Huang, Y.; Yang, Q.; Liu, S.; Wang, J.; Du, P.; Cheng, X.; Zhou, Z. Research on the Improvement of Concrete Autogenous Self-healing Based on the Regulation of Cement Particle Size Distribution (PSD). *Materials* **2019**, *12*, 2818. [CrossRef]
72. Beglarigale, A.; Eyice, D.; Tutkun, B.; Yazıcı, H. Evaluation of enhanced autogenous self-healing ability of UHPC mixtures. *Constr. Build. Mater.* **2021**, *280*, 122524. [CrossRef]
73. Tomczak, K.; Jakubowski, J.; Kotwica, Ł. Enhanced autogenous self-healing of cement-based composites with mechanically activated fluidized-bed combustion fly ash. *Constr. Build. Mater.* **2021**, *300*, 124028. [CrossRef]
74. Kim, D.J.; Kang, S.H.; Ahn, T.H. Mechanical Characterization of High-Performance Steel-Fiber Reinforced Cement Composites with Self-Healing Effect. *Materials* **2014**, *7*, 508–526. [CrossRef]
75. Reddy, T.C.S.; Ravitheja, A.; Sashidhar, C. Micromechanical Properties of Self-Healing Concrete with Crystalline Admixture and Silica Fume. *ACI Mater. J.* **2020**, *117*, 63–74. [CrossRef]

76. Suleiman, A.R.; Nehdi, M.L. Effect of autogenous crack self-healing on mechanical strength recovery of cement mortar under various environmental exposure. *Sci. Rep.* **2021**, *11*, 7245. [CrossRef] [PubMed]
77. Van Mullem, T.; Anglani, G.; Dudek, M.; Vanoutrive, H.; Bumanis, G.; Litina, C.; Kwiecień, A.; Al-Tabbaa, A.; Bajare, D.; Stryszewska, T.; et al. Addressing the need for standardization of test methods for self-healing concrete: An interlaboratory study on concrete with macrocapsules. *Sci. Technol. Adv. Mater.* **2020**, *21*, 661–682. [CrossRef]
78. Tsangouri, E.; Lelon, J.; Minnebo, P.; Asaue, H.; Shiotani, T.; Van Tittelboom, K.; De Belie, N.; Aggelis, D.G.; Van Hemelrijck, D. Feasibility study on real-scale, self-healing concrete slab by developing a smart capsules network and assessed by a plethora of advanced monitoring techniques. *Constr. Build. Mater.* **2019**, *228*, 116780. [CrossRef]
79. Feng, J.; Dong, H.; Wang, R.; Su, Y. A novel capsule by poly (ethylene glycol) granulation for self-healing concrete. *Cem. Concr. Res.* **2020**, *133*, 106053. [CrossRef]
80. Qureshi, T.S.; Kanellopoulos, A.; Al-Tabbaa, A. Encapsulation of expansive powder minerals within a concentric glass capsule system for self-healing concrete. *Constr. Build. Mater.* **2016**, *121*, 629–643. [CrossRef]
81. Li, Y.; Yu, J.; Cao, Z.; He, P.; Liu, Q.; Han, X.; Wan, Y. Preparation and application of novel microcapsules ruptured by microwave for self-healing concrete. *Constr. Build. Mater.* **2021**, *304*, 124616. [CrossRef]
82. Wang, J.; Dewanckele, J.; Cnudde, V.; Van Vlierberghe, S.; Verstraete, W.; De Belie, N. X-ray computed tomography proof of bacterial-based self-healing in concrete. *Cem. Concr. Compos.* **2014**, *53*, 289–304. [CrossRef]
83. Singh, H.; Gupta, R. Cellulose fiber as bacteria-carrier in mortar: Self-healing quantification using UPV. *J. Build. Eng.* **2020**, *28*, 101090. [CrossRef]
84. Mousavi, S.S.; Guizani, L.; Bhojaraju, C.; Ouellet-Plamondon, C. The effect of air-entraining admixture and superabsorbent polymer on bond behaviour of steel rebar in pre-cracked and self-healed concrete. *Constr. Build. Mater.* **2021**, *281*, 122568. [CrossRef]
85. Xiao, X.; Ho, D.S.W.; Yang, E.H. The use of low alkalinity MgO-SiO2 formulation to encapsulate bacteria for self-healing concrete. *Constr. Build. Mater.* **2023**, *401*, 132908. [CrossRef]
86. Du, W.; Yu, J.; Gu, S.; Wang, R.; Li, J.; Han, X.; Liu, Q. Effect of temperatures on self-healing capabilities of concrete with different shell composition microcapsules containing toluene-di-isocyanate. *Constr. Build. Mater.* **2020**, *247*, 118575. [CrossRef]
87. Sisomphon, K.; Çopuroğlu, O.; Fraaij, A. Application of Encapsulated Lightweight Aggregate Impregnated with Sodium Monofluorophosphate as a Self-Healing Agent in Blast Furnace slag Mortar). 2011. Available online: https://repository.tudelft.nl/record/uuid:989836d6-dd5c-4bb0-8d9f-925390dddbae (accessed on 5 May 2025).
88. MacLaren, D.C.; White, M.A. Cement: Its Chemistry and Properties. *J. Chem. Educ.* **2003**, *80*, 623–635. [CrossRef]
89. Kutchko, B.G.; Strazisar, B.R.; Dzombak, D.A.; Lowry, G.V.; Thauiow, N. Degradation of well cement by CO_2 under geologic sequestration conditions. *Environ. Sci. Technol.* **2007**, *41*, 4787–4792. [CrossRef]
90. Nygaard, R. *Well Design and Well Integrity: Wabamun Area CO_2 Sequestration Project*; University of Calgary: Calgary, AB, Canada, 2010; Available online: https://www.ucalgary.ca/wasp/Well%20Integrity%20Analysis.pdf (accessed on 5 March 2025).
91. Abid, K.; Gholami, R.; Choate, P.; Nagaratnam, B.H. A review on cement degradation under CO_2-rich environment of sequestration projects. *J. Nat. Gas Sci. Eng.* **2015**, *27*, 1149–1157. [CrossRef]
92. Ahmed, A.; Mahmoud, A.A.; Elkatatny, S.; Chen, W. The Effect of Weighting Materials on Oil-Well Cement Properties While Drilling Deep Wells. *Sustainability* **2019**, *11*, 6776. [CrossRef]
93. Wang, L.; He, Z.; Cai, X. Characterization of pozzolanic reaction and its effect on the C-S-H gel in fly ash-cement paste. *J. Wuhan Univ. Technol. Mater. Sci. Ed.* **2011**, *26*, 319–324. [CrossRef]
94. Duguid, A.; Radonjic, M.; Bruant, R.; Mandecki, T.; Scherer, G.; Celia, M. The effect of CO_2 sequestration on oll well cements. In *Greenhouse Gas Control Technologies 7*; Elsevier: Oxford, UK, 2005; pp. 1997–2001. [CrossRef]
95. Geological. In *PHREEQC Version 3 | U.S. Geological Survey*. Available online: https://www.usgs.gov/software/phreeqc-version-3 (accessed on 11 April 2025).
96. Geloni, C.; Giorgis, T.; Battistelli, A. Modeling of Rocks and Cement Alteration due to CO_2 Injection in an Exploited Gas Reservoir. *Transp. Porous Media* **2011**, *90*, 183–200. [CrossRef]
97. Szabó-Krausz, Z.; Gál, N.E.; Gável, V.; Falus, G. Wellbore cement alteration during decades of abandonment and following CO_2 attack—A geochemical modelling study in the area of potential CO_2 reservoirs in the Pannonian Basin. *Appl. Geochem.* **2020**, *113*, 104516. [CrossRef]
98. Wasch, L.J.; Koenen, M.; Wollenweber, J.; Tambach, T.J. Sensitivity of chemical cement alteration—Modeling the effect of parameter uncertainty and varying subsurface conditions. *Greenh. Gases Sci. Technol.* **2015**, *5*, 323–338. [CrossRef]

Disclaimer/Publisher's Note: The statements, opinions and data contained in all publications are solely those of the individual author(s) and contributor(s) and not of MDPI and/or the editor(s). MDPI and/or the editor(s) disclaim responsibility for any injury to people or property resulting from any ideas, methods, instructions or products referred to in the content.